Review

Performance Improvement Overview of the Supercritical Carbon Dioxide Brayton Cycle

Xurong Wang [1,2], Longwei Zhang [2], Zhenhua Zhu [3], Mingjiang Hu [1], Jing Wang [1] and Xiaowei Fan [1,*]

[1] School of Energy and Building Environment Engineering, Henan University of Urban Construction, Pingdingshan 467036, China; xurong.wang@huuc.edu.cn (X.W.)
[2] School of Energy and Power Engineering, Shandong University, Jinan 250061, China
[3] School of Energy and Environment, Zhongyuan University of Technology, Zhengzhou 451191, China
[*] Correspondence: fxw@huuc.edu.cn

Abstract: Efficiency and compactness are core strengths of the supercritical carbon dioxide (sCO_2) Brayton cycle, which is considered an alternative to the steam Rankine cycle for moderate-temperature heat sources (350–800 °C). Numerical investigations on system design and analysis have received considerable attention, with the aim of improving the sCO_2 cycle from the viewpoint of thermodynamics. This paper reviews and compares previous studies in the literature to survey different cycle layouts, operating parameters, and working fluids of the sCO_2 cycle. Performance enhancement approaches are categorized into three classes according to characteristics: conventional methods, CO_2 mixtures, and combined cycles. The strengths, weaknesses, and limitations of each categorized method are discussed. This research is expected to provide a roadmap for performance improvement that meets the interests of researchers.

Keywords: supercritical carbon dioxide cycle; performance improvement; review; combined cycle; binary mixture

1. Introduction

The supercritical carbon dioxide (sCO_2) Brayton cycle employs supercritical CO_2 working fluid for electricity generation and is characterized by high cycle efficiency, small turbomachinery, high power density, and a simple cycle layout. This emerging technology is adaptable to the majority of heat sources, such as nuclear, solar, fossil fuels, and waste heat, and has attracted significant attention in the last couple of decades [1]. Figure 1 presents publication numbers on a yearly basis with respect to this hot topic since 2002. A body of raw data was collected by Wang [2]. The number of annual publications has risen exponentially. The number of articles published by Chinese researchers has grown since 2014. In 2019, China published more than 80 studies, which accounted for 36.6% of the total documented in an international journal and conference database. Research on nuclear power plants accounts for 42.9% of all sCO_2 cycle research reported in the literature, followed by research on concentrating solar power (CSP) (30.2%) and waste heat recovery (WHR) from gas turbines (9.6%) and fossil power plants (8.2%). Currently, research on the sCO_2 cycle is in the experimental and demonstration stages. The net power tests a 50 MWth plant to demonstrate the zero-emission Allam cycle, which is a variant of the sCO_2 cycle [3]. The Supercritical Transformational Electric Power (STEP) project is being developed by the Southwest Research Institute (SwRI), Gas Technology Institute (GTI), GE Global Research (GE), and the U.S. Department of Energy (DOE) to operate a 10 MWe indirect-fired sCO_2 cycle [4]. In Europe, components have been designed and tested for the sCO2-HeRo (supercritical CO_2 heat removal system), which is considered a backup cooling system for the reactor core [5]. In China, the Institute of Engineering Thermophysics (IET) built an MW-scale sCO_2 compressor test platform to demonstrate CO_2 compression under subcritical and supercritical conditions [6]. In addition, a printed circuit heat exchanger

facility is under development by the IET, with CO_2 operating at a temperature and pressure of 550 °C and 32 MPa, respectively [7].
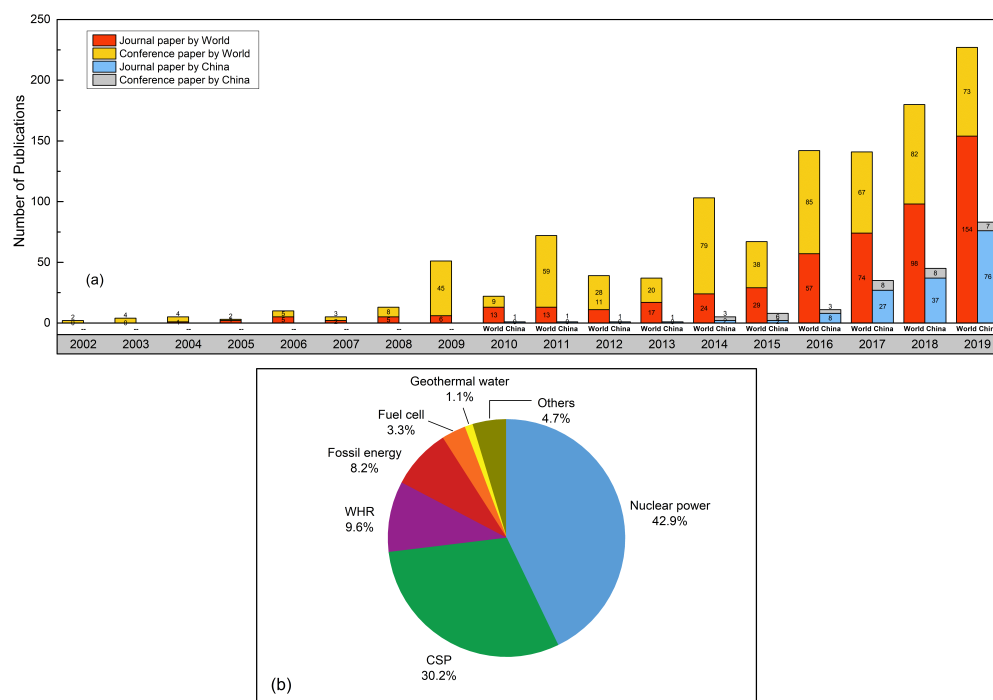
Figure 1. Research on the sCO_2 cycle from 2002 to 2019. (**a**) Annual publications. (**b**) Application share.

Compression near the critical point of CO_2 benefits the thermal efficiency of the sCO_2 cycle, but also constrains the application. Power plants operating in hot and/or arid environments are not uncommon, especially for CSP in deserts, taking advantage of the excellent year-round solar radiation. High ambient air temperatures in the range of 25–37 °C [8] and dry air-cooling technologies make it difficult and costly to achieve the desired condition at the inlet of the compressor. High compressor inlet temperatures (CITs) considerably reduce the thermal efficiency of the sCO_2 cycle [9]. In addition, daily and seasonal variations of heat sources and cooling conditions or the use of inefficient cooling systems can hinder the performance of the sCO_2 cycle. A cycle design with low CITs leads to long periods of part-load operation, whereas a high-temperature design penalizes the cycle efficiency [10,11].

Increasing the thermal efficiency of the sCO_2 cycle and the design of new cycles are among the interests of researchers in the field of thermodynamics. Moisseytsev and Sienicki [12] reported several improved methods for the sCO_2 cycle heated by a sodium-cooled fast reactor (SFR). These methods include broad operating ranges (temperature and pressure) and modifications of cycle configuration (reheating, intercooling, recompression, and condensation). Ahn et al. [13] reported on development progress with respect to the sCO_2 cycle and compared single-flow and split-flow cycle layouts. Crespi et al. [14] reviewed and categorized sCO_2 cycles according to their configurations, covering 42 varieties of stand-alone cycles and 38 combined layouts. However, they failed to present details of performance enhancement or include studies on the CO_2 mixture Brayton cycles. Li et al. [15] summarized the development of the sCO_2 cycle in the nuclear and solar industries and categorized designs into single-flow and split-flow layouts. They covered improvement in sCO_2 cycles (like using a bottoming cycle) but focused on the research status rather than the comparison of performance improvement. Wang et al. [16] reviewed and compared six sCO_2 cycles for solar tower CSP. Xu et al. [17] focused on barriers to current research on the sCO_2 cycle.

The research gap lies in a lack of a comprehensive review and interpretation of performance improvement options for the sCO$_2$ cycle, as well as a comparison of enhanced thermal efficiencies and analysis of the limitations of each method. CO$_2$ mixtures were previously employed to adjust the critical point of pure CO$_2$ for power cycles adapting to higher or lower heat sinks [18]. The features and influence of this approach may be aggressive or moderate with respect to other methods. It is not possible to draw a conclusion as to which method is preferable without comparison. In the present paper, we review previously published papers published on methods that could enhance the sCO$_2$ cycle. Applications, cycle layouts, methods, claimed thermal efficiencies, and operating conditions are presented. Each approach is interpreted and categorized according to its type and characteristics. the claimed performance changes of the sCO$_2$ cycle are compared from the viewpoints of thermodynamics and economics. In addition, we discuss the strengths, weaknesses, and limitations of each categorized method. This research is expected to provide an intuitive overview of the performance enhancement of sCO$_2$ cycles.

2. Conventional Method

A conventional method is referred to as a classical approach to improve a power cycle, such as with intercooling, reheating, recuperation, and high operating parameters, which have been applied to the Rankine cycle and Brayton cycle. In the early stages, these options were considered to be handy and extensive. Figure 2 presents four popular schematic diagrams of the sCO$_2$ cycle layout that have been improved by using the conventional method. Angelino [19] studied the various layouts of the sCO$_2$ cycle. However, he mainly focused on the transcritical CO$_2$ (tCO$_2$) cycle, i.e., the condensation cycle. Later, intercooling, reheating, recompression, partial cooling, and precompression were investigated [9,20–22]. Table 1 summarizes the methods, boundary conditions, and thermal efficiencies declared in the literature. It should be noted that these studies are theoretical and are based on specific component efficiency assumptions, forming many varieties of the sCO$_2$ cycle, as reviewed by Crespi et al. [14]. Since a heat exchanger contributes 54% to the capital cost of the recompression of the sCO$_2$ cycle [23], a reduction in pressure loss and the enhancement of heat transfer play important roles in enhancing the performance of the sCO$_2$ cycle from the point of view of exergy and energy [24–26]. This is also true for an increase in turbomachinery efficiency. The reason why Table 1 does not list the improved methods of the components is that these methods are less important than the cycle layout modifications and operating parameters.
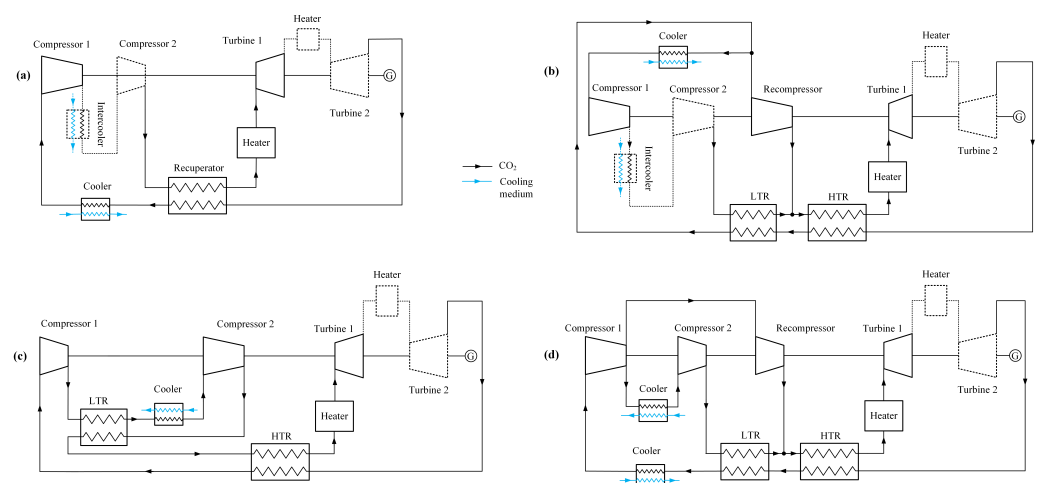
Figure 2. The alternative sCO$_2$ cycle layouts. (**a**) Recuperated cycle. (**b**) Recompression cycle. (**c**) Precompression cycle. (**d**) Partial cooling cycle.

Table 1. Numerical study on varied sCO$_2$ cycles enhanced by the conventional method.

Cycle Layout	Initial Behavior				Improved Behavior		Application	Ref.
	CIT/°C	TIP/MPa	TIT/°C	η/%	Method	η/%		
Intercooled Recuperated	31	22	550	39	Recompression, Increase TIT	41.8–47	300 MWe Nuclear power	2002 [27]
Recompression	31	20	550	43.1, 45.8	Increase TIT	47, 49.9	600 MWth Nuclear power	2002 [27]
Recuperated	32	20	550	40	Reheating, Intercooling	40.8–41.5	600 MWth Nuclear power	2004 [9]
Recompression	32	20	550–750	45.56–52	Reheating, Increase TIT, Raise TIP	46.775–57	600 MWth Nuclear power	2004 [9]
Recuperated	35	7, 12	800	45.5, 45.8	Intercooling, Partial cooling	47.4–49.7	Nuclear power	2004 [20]
Partial cooling	35	7, 12	800	49.2, 49.7	Intercooling	51.4, 51.9	Nuclear power	2004 [20]
Recompression	31.25	20	472	39.1	Condensation, Liquid phase pumping, Raise TIP	39.5–43.1	250 MWth Nuclear power	2007 [12]
Recompression	32, 50	20, 30	550, 750	36.71–49.83	Reheating	37.65–50.78	600 MWth Nuclear power	2009 [28]
Recuperated	32	25	550–750	40.44–48.2	Precompression, Recompression, Partial cooling, Increase TIT	43.49–54.1	3600 MWth Nuclear power	2011 [29]
Precompression	32	25	550	43.49	Increase TIT	48.8, 52.4	3600 MWth Nuclear power	2011 [29]
Recompression	32	25	550	46.48	Increase TIT	49.9, 52.7	3600 MWth Nuclear power	2011 [29]
Partial cooling	32	25	550	46.12	Increase TIT	50.5, 54.1	3600 MWth Nuclear power	2011 [29]
Recuperated	32	25	550–700	40.7–45.5	Reheating, Increase TIT, Recompression, Partial cooling	42.5–52.8	CSP	2012 [30]
Recompression	32	25	550–700	47.7–52.8	Reheating, Increase TIT	48.9–53.9	CSP	2012 [30]
Partial cooling	32	25	550–700	46.1–52	Reheating, Increase TIT	48.1–53.8	CSP	2012 [30]
Recompression	32	25	500–600	44.5–46	Reheating, Increase TIT	47–49	10 MWe CSP	2012 [31]
Recompression	55.5	25	500–850	40–52	Reheating, Increase TIT	43.14–52.8	CSP	2015 [32]
Recuperated	55.5	25	600	38.5	Reheating, Recompression	39.5, 42.7	CSP	2015 [33]
Recompression	55.5	25	600	42.7	Reheating, Intercooling	43.2–45.3	CSP	2015 [33]
Recompression	32	25	600–800	45.1–52.4	Reheating, Increase TIT	46.5–53.4	2113 MWth Fossil energy	2016 [34]
Recompression	35, 50	20	500–800	39.59–54.58	Intercooling	40.82–55.68	Nuclear power	2017 [21]
Recuperated with reheating	27	25	827	46.3	Intercooling	48.7–49.4	160 MWe Not specified	2017 [35]
Recuperated	-	25	700	36.2	Recompression, Precompression	43.3	104 MWe CSP	2017 [22]
Recompression with reheating	32	25	500	40.98–49.21	Intercooling	41.44–49.4	50 MWe CSP	2017 [36]
Recompression	51	25	750	47	Intercooling	48.6	25 MWe CSP	2017 [37]

Figure 3 shows the thermal efficiency of enhanced sCO_2 cycles as a function of turbine inlet temperature (TIT). Note that the efficiencies of various configurations were collected from published papers on the basis of very different boundary conditions. In order to establish a convincing comparison, the commonly used efficiencies of the sCO_2 cycle were plotted as the reference [9]. It is noted that the reference data were calculated without consideration of cycle losses. It can be seen that the enhanced recuperated sCO_2 cycle has an efficiency in the order of about 3% lower than the reference efficiency at the same TIT. The efficiencies of the improved recompression and partial cooling cycles are higher than the reference efficiencies, except for several points. This is mainly due to high CITs for these cycles, such as 50 °C [28], 51 °C [37], and 55.5 °C [32,33]. Figure 3 also presents the recompression cycle with thermal efficiencies of up to 50% at a TIT of 500 °C. This was achieved not only by reheating but also by the combination of intercooling, high-efficiency turbomachinery, and large recuperator conductance [36,38].

Figure 4 shows the cycle efficiency improvement at various TITs for each specific conventional method. Note that the improvements in efficiency achieved by the reheating or intercooling is obtained with respect to the sCO_2 cycle without modification. As for the methods for the CO_2 condensation cycle, CO_2 liquid-phase pumping, precompression, recompression, and partial cooling, the improvement in efficiency is the efficiency difference for the recuperated sCO_2 cycle. Efficiency gains from increasing TITs are calculated for every 100 °C rise in the TIT. Moreover, the turbine inlet pressure (TIP) is also a crucial factor in changing the efficiency.
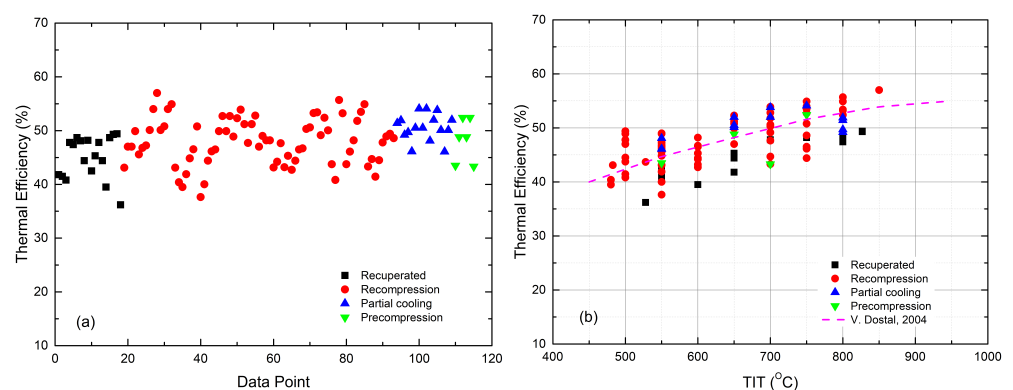
Figure 3. The thermal efficiency of modified sCO_2 cycles listed in Table 1. (**a**) Summary of global thermal efficiencies. (**b**) Improved thermal efficiency as a function of TIT [9].

For the sCO_2 cycle, the typical conditions at the turbine inlet are 550 °C and 20 MPa [9,39]. It is known that a higher temperature or pressure implies higher cycle efficiency. Figure 4 shows that an order of about 4% additional efficiency is obtained for each 100 °C rise in the TIT. At higher TITs, the efficiency improvement diminishes to 3% [9]. When increasing the TIT from 550 °C to 650 °C, efficiency was improved by 2.8% and 4% for the recuperated (with intercooling) and recompression sCO_2 cycles, respectively [27]. For a precompression layout with higher turbomachinery performance, increasing the temperature to 650 °C improved the efficiency by 5.3% to a value of 48.8% [29]. As for TIPs beyond 20 MPa, the gain in cycle efficiency is very modest. About a 0.3% increase in cycle efficiency was achieved when the TIP was raised from 20 to 22 MPa (at a TIT of 480 °C) [12]. Dostal [9] showed that increasing the pressure from 20 to 25 MPa yielded 1.4% (at a TIT of 650 °C) and 2.0% (at a TIT of 750 °C) efficiency improvements. In contrast, the increase in efficiency was less than 1% when the TIP rose from 25 MPa to 30 MPa. It should be noted that higher temperature and/or pressure conditions represent challenges in terms of material selection. Raising the pressure means increasing the thickness of the pipes, pressure-bearing casings, and heat exchangers, requiring additional capital costs. Moreover, material corrosion should be considered in high turbine inlet conditions.
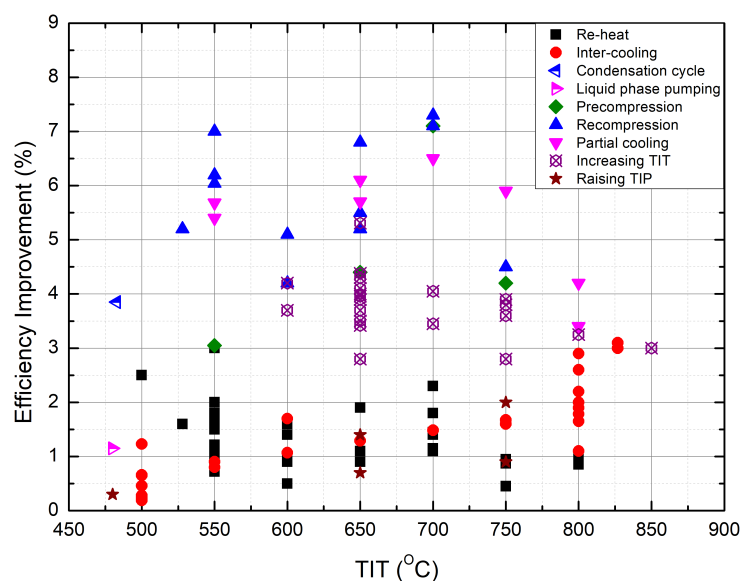
Figure 4. Efficiency improvement of the sCO$_2$ cycle enhanced by the conventional method.

The sCO$_2$ cycle takes advantage of the non-ideal properties of CO$_2$ near the critical point to reduce the compression work. It was shown that higher cycle efficiency could be obtained if the CO$_2$ is cooled below the pseudocritical temperature at a given supercritical pressure. When the temperature declines across the critical point, the cycle is called the "CO$_2$ liquid cycle" or "CO$_2$ condensation cycle", depending on the compressor inlet pressure crossing the critical point (the latter) or not (the former). The liquid-phase cycle operating at supercritical pressures increased the thermal efficiency by 1.15% at pump inlet conditions of 30 °C and 7.4 MPa [12]. The CO$_2$ condensation cycle (under pump inlet conditions of 20 °C and 5.75 MPa) achieved an efficiency of 43.1% for a 483 °C SFR, having an efficiency improvement of 3.85% [12]. These two cycles should be carefully treated due to the requirement of a year-round supply of the cold-cooling medium. Moreover, in order to cool CO$_2$ below the critical temperature, the CO$_2$ has to pass through the peak specific heat, resulting in a significant increase in the heat transfer area of the cooler.

Reheating improves thermal efficiency by increasing the equivalent Carnot temperature, i.e., the average temperature at which the heat is added to the power cycle. As shown in Figure 4, reheating adds 1–2% to the thermal efficiency. The gains provided by a second reheating configuration, when compared to single reheating, stay below 0.5% and lower at high TITs [9,30,34]. Figure 4 also shows that single-stage reheating could obtain a 2.5% and 3.0% increase in efficiency at TITs of 500 °C and 550 °C, respectively, resulting from a high TIP of 25 MPa and a better component performance [31]. Several factors should be paid attention to regarding the reheating method: (1) The effect of reheating strongly depends on the pressure drop through the reheater. With an increase in pressure drop, the benefit from the reheat decreases until it is negative [9,33]. (2) In contrast to an ideal gas cycle, the pressure ratio split between sCO$_2$ turbines should be optimized to give equivalent temperatures of heat addition. It was observed that the optimum pressure–ratio split was slightly lower than an equal split [9]. (3) It was shown that using more than one stage of reheating is economically unattractive [9].

Intercooling reduces the average temperature of heat rejection from the sCO$_2$ cycle. However, the CO$_2$ compression work is already low, such that the benefit from intercooling is expected to be limited. As shown in Figure 4, intercooling offers a very modest efficiency improvement, which was 0.8% at a TIT of 550 °C (recuperated sCO$_2$ layout) [9]. With a significant increase in the TIT, the efficiency is slightly increased. It can be seen that efficiency gains can be up to 3% at TITs of higher than 800 °C [20,35]. This is due to the existence of large compression work in the original sCO$_2$ cycle. It should be noted that the properties of CO$_2$ are considerably affected by the critical point, and thus, the

pressure–ratio split is not equal in order to achieve the same TIP. It was shown that the second compressor provided a 1.5 to 1.9 times higher pressure ratio than the equally split pressure ratio, giving the best cycle performance [9,21]. An equal pressure ratio for the two compressors results in a slightly low thermal efficiency [12]. The disadvantage of intercooling is the additional cost.

The cause of the irreversibility of the recuperator is the pinch-point problem, which largely reduces the performance of the sCO$_2$ cycle. In order to overcome this problem, compound cycles were introduced [19]. The precompression cycle is another way to increase regeneration [9,40]. As reported in [29], this cycle layout achieved an efficiency improvement of 4% over the recuperated sCO$_2$ cycle. The partial cooling cycle operates at pressures of about 12 MPa and temperatures of around 700–800 °C. Its efficiency is improved by reducing the average temperature of heat rejection. As can be seen in Figure 4, the efficiency improvement from the partial cooling cycle is larger than that from the precompression cycle. The recompression cycle improves efficiency by reducing the heat rejection from the cycle using an additional compressor before the cooler. The efficiencies of complex cycles (recompression and partial cooling) are consistently about 6% higher than those of the recuperated cycle [30]. At high CITs, the efficiency increase is reduced to a grade of around 4% [20,33].

3. Combined Cycle

Although the sCO$_2$ cycle has promising thermal efficiency, about 50% of heat addition is still rejected to the heat sink at temperatures of 100 °C to 200 °C. For the purpose of minimizing thermodynamic irreversibility as a consequence of the second law, WHR technologies were employed in the sCO$_2$ cycle either for power generation or cold supply [2,14]. The WHR technology, or a bottoming cycle, is introduced between the low-temperature recuperator (LTR) and the cooler with an additional heat exchanger, as shown in Figure 5. This approach is recognized as the combined cycle method, by which the recuperator in the topping cycle does not need to have high effectiveness. Table 2 presents the different configurations of the sCO$_2$ combined cycle in the literature. The bottoming cycles considered are the organic Rankine cycle (ORC), tCO$_2$ cycle, and the Kalina cycle. Statistics show that about 56% of combined sCO$_2$ cycles use the ORC bottoming cycle, and 38% employ the tCO$_2$ cycle. Only two papers are devoted to the complicated Kalina cycle. It should be noted that the combined cycle method requires a year-round supply of very cold cooling water. The WHR technologies operate at narrow temperature ranges between the heat source and heat sink. The working fluid needs a condensation process to maintain higher performance.

Figure 6 plots the declared thermal efficiencies of the combined sCO$_2$ system in the literature. Wide dispersion is observed in the chart, showing global efficiencies in the range of 35% to 60%. This is due to the layout and boundary conditions of each combined cycle, as shown in Table 2. The efficiencies, as well as the reference efficiencies, of the stand-alone sCO$_2$ cycle [9] are further plotted against TIT in Figure 6, showing the clear influence of this parameter on the performance of the combined cycle. The thermal efficiencies of the combined recuperated cycles are nearly 5% lower than reference efficiencies. Figure 7 shows the efficiency improvement after adding a bottoming cycle to the sCO$_2$ cycle at various TITs. In order to show more details, three common layouts of the topping sCO$_2$ cycle are distinguished using symbols and colors. The efficiency improvement is defined as the thermal efficiency of the combined sCO$_2$ cycle over the thermal efficiency of the initial sCO$_2$ cycle.

$$\eta_{initial} = \frac{W_{net,sCO_2}}{Q_{in}} \tag{1}$$

$$\eta_{combined} = \frac{W_{net,topping} + W_{net,bottom}}{Q_{in}} \tag{2}$$

$$\eta_{improvement} = \eta_{combined} - \eta_{initial} \tag{3}$$

Table 2. Numerical study on sCO$_2$ combined cycles.

Cycle Layout	Initial Behavior					Improved Behavior			Application	Ref.
	CIT/°C	TIP/MPa	TIT/°C	η/%	Cost	Bottoming Cycle	η/%	Cost		
Recompression	32	22.3	550–750	40.23–47.82	-	tCO$_2$ cycle	44.25–52.98	-	90–165 kWe nuclear power	2010 [41]
Recuperated	35	22.5	527–727	28.5–33.8	-	ORC (R245fa, isobutane, isopentane, cyclohexane)	36.4–43.96	-	88–115 kWe CSP	2011 [42]
Recuperated	30	-	527–827	28.1–38.7	-	ORC (isopentane, isobutane, n-Butane)	35.3–47.5	-	500 kWe CSP	2013 [43]
Recuperated	55	25	700–850	41.9–46.5	-	ORC (isopentane, n-butene, cis-butene)	48–53	-	CSP	2014 [44]
Recompression	55	25	700-850	46.3–50.6	-	ORC (R236ea, R245fa, isobutane)	50.5–55.75	-	CSP	2014 [44]
Partial cooling	55	25	700-850	46.2–51	-	ORC (R124, R245fa, isobutane)	48.7–53.95	-	CSP	2014 [44]
Recuperated	35	22.5	650	33.8, 36.5	-	tCO$_2$ cycle	39.5, 41.3	-	326 kWth Fuel cell	2014 [45]
Recuperated	35	22.5	650	39.6	-	tCO$_2$ cycle	46.1	-	326 kWth Fuel cell	2014 [46]
Recompression	35	20	527	45.32	-	ORC (R123)	52.12	-	570 kWth Nuclear power	2014 [47]
Recompression	35	22.2	550	39.59, 38.3	11.2 $/GJ, 10.87 $/GJ	ORC (Isopentane, n-butane, isobutane, n-pentane, R123, R114, R141b, RC318)	43.68–44.22	10.73 $/GJ, 10.25 $/GJ	600 MWth Nuclear power	2014 [48]
Recompression	32	20	550	44.29	6.2 $/kW	tCO$_2$ cycle	45.92	6.6 $/kW	84 kWe Nuclear power	2015 [23]
Recuperated	32	20	550	37.46	-	tCO$_2$ cycle	44.7	-	96 kWe Nuclear power	2015 [49]
Recompression	32	20	550	44.22	-	tCO$_2$ cycle	47.69	-	81 kWe Nuclear power	2015 [49]
Recompression	32	26.7, 21	550	-	-	tCO$_2$ cycle	44.99, 43.89	9.98 $/GJ, 9.75 $/GJ	600 MWth Nuclear power	2016 [50]
Recompression	32	28.12–29.53, 20.87–21.16	550	-	-	ORC (R123, R245fa, toluene, isobutane, isopentane, cyclohexane)	44.77–45.23, 43.78–44.08	9.88–9.96 $/GJ, 9.60–9.62 $/GJ	600 MWth nuclear power	2016 [50]
Recompression	35	21.5	550	39.57	11.2 $/GJ, 10.87 $/GJ	Kalina cycle	43.55	10.73 $/GJ, 10.34 $/GJ	600 MWth Nuclear power	2016 [51]
Recompression	35	22	550	39.62	13.73 $/GJ, 13.64 $/GJ	Kalina cycle	42.8	13.04 $/GJ, 12.88 $/GJ	600 MWth Nuclear power	2016 [52]
Recuperated	37	-	655	-	-	ORC (R245fa)	-	0.039 cents/kWh, 0.045 cents/kWh	Fuel cell	2016 [53]
Recompression	33	-	550	-	-	tCO$_2$ refrigeration	49.9–50.52	10.68–11.05 $/GJ	600 MWth Nuclear power	2017 [54]
Basic	32.5	20	385	51.41	-	tCO$_2$ cycle	52.53	-	9.25 MWe Exhaust gas	2017 [55]
Recompression	31	21.2	501.8	37.68	-	tCO$_2$ cycle	50.06	0.046 $/kWh	41.45 MWe Exhaust gas	2017 [56]
Recompression	32	20	550	41.47	-	tCO$_2$ cycle	43.75	11,243.15 $/h	600 MWth Nuclear power	2017 [57]
Recompression	32	-	600–850	44.5–51.9	-	tCO$_2$ cycle	47.6–57.1	-	2.7–4.2 MWe Not specified	2018 [58]
Recompression	32	-	750	-	-	ORC (10 zeotropic mixtures)	-	10.93 $/GJ	600 MWth nuclear power	2018 [59]
Recuperated	31	31.06	450.6	-	-	ORC (cyclopentane/R365mfc)	-	3.95–4.34 cents/kWh	Exhaust gas	2018 [60]
Recuperated	40	20	550	-	-	tCO$_2$ refrigeration	42.3–44.5	-	2.4–3.0 MWe Exhaust gas	2018 [61]
Recuperated	-	25	380	-	-	ORC (R407c, R134a, R245fa, R1234yf, R1234ze)	40.5–41.92		3.4–3.7 MWe CSP	2018 [62]
Recuperated, recompression	36	16.4	300	-	-	ORC (R123, R245fa, R600)	17.7–19.1	-	200 kWe Not specified	2018 [63]
Basic	52–55	20	385	-	-	tCO$_2$ cycle	49.39–51.44	0.042–0.0486 $/kWh	8.886–9.255 MW Exhaust gas	2018 [64]
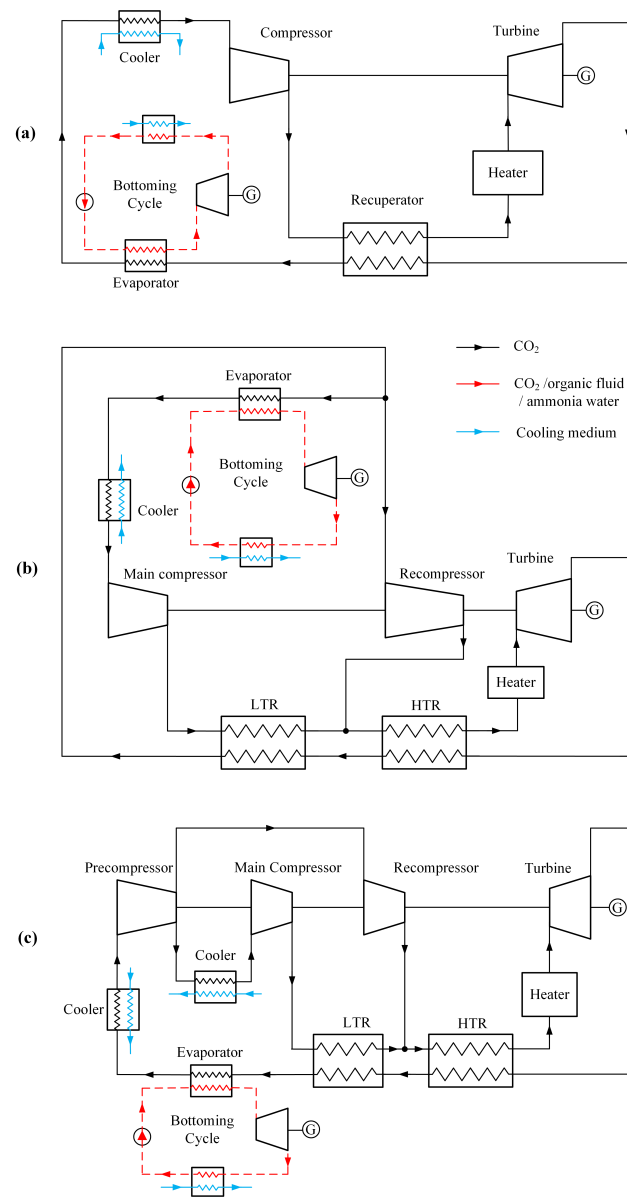
Figure 5. The combined sCO$_2$ cycle layouts. (**a**) Combined recuperated cycle. (**b**) Combined recompression cycle. (**c**) Combined partial cooling cycle.
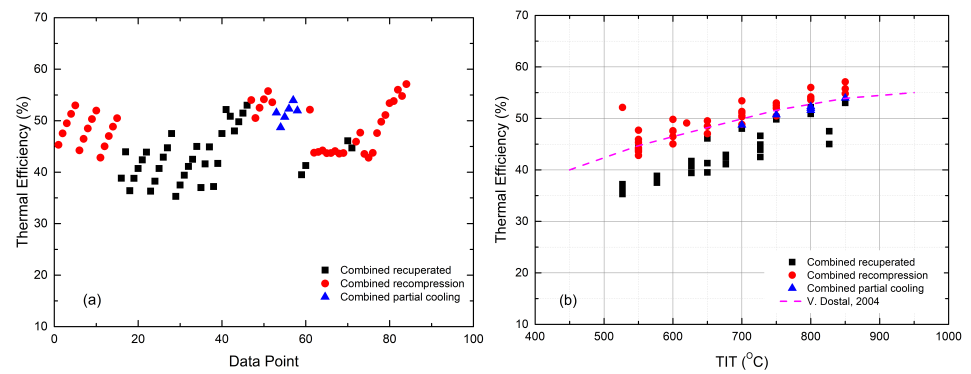
Figure 6. Thermal efficiency of combined sCO$_2$ power cycles listed in Table 2. (**a**) Improved thermal efficiencies. (**b**) Global thermal efficiencies as functions of TIT [9].
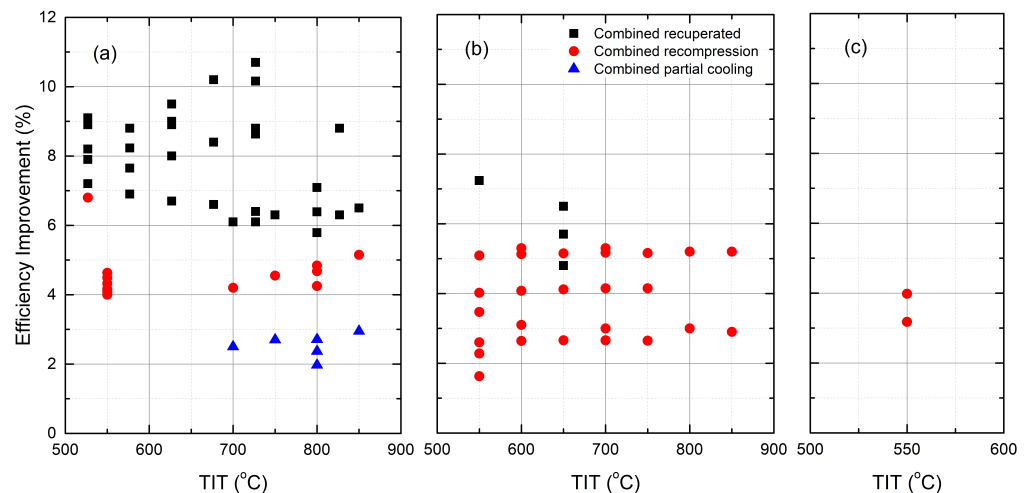
Figure 7. The sCO$_2$ cycle thermal efficiency improvement with the combined cycle method. (**a**) +ORC. (**b**) +tCO$_2$ cycle. (**c**) +Kalina cycle.

ORC employs a refrigeration fluid as the working fluid to convert low-temperature heat into electricity, and this is applicable to the heat sources of geothermal energy [65], solar energy [66], and industrial waste heat [67–69]. There is an established industry with over 2000 MW installed. ORC technology was first added to a recuperated sCO$_2$ cycle (operating at the turbine inlet conditions of 727 °C and 30 MPa) in 2008, showing that the efficiency was improved by 6.1% when using cyclohexane as the working fluid [70]. Some interesting information from the literature review can be found as follows:

- ORC is mainly combined with the recuperated sCO$_2$ cycle, followed by the recompression and partial cooling cycles. The recuperated sCO$_2$-ORC combined cycle is slightly less complex than the other two combined cycles. Moreover, the recuperated sCO$_2$ cycle has a relatively larger amount of waste heat at high temperatures, which is the ideal source for WHR technologies.

- The performance of the recuperated sCO$_2$ cycle is significantly improved by the additional ORC cycle. As shown in Figure 7, the gain in efficiency ranges from 6 to 13%, which is achieved by the combined cycle compared to the stand-alone recuperated sCO$_2$ cycle [42]. The CIT and organic fluid are the main contributors to the diversity of performance enhancement [44]. For the recompression sCO$_2$ cycle, the efficiency was improved by 4–4.6% at a TIT of 550 °C [48] and 4.2–5% at a TIT of higher than 700 °C [44]. Zhang et al. [47] studied a recompression sCO$_2$-ORC combined cycle, having a thermal efficiency of 52.12% when using a liquefied natural gas (LNG) as the heat sink. About 6.8% of additional efficiency was achieved with respect to the stand-alone cycle due to the small power scale, i.e., 297 kWe, of which the bottoming cycle output accounted for 13%. As for the partial cooling sCO$_2$ cycle, the gain in efficiency ranged from 2–3% [44] depending on organic fluids.

- The recompression sCO$_2$-ORC cycle achieves the highest overall efficiency. It can be seen from Figure 6 that most combined recompression cycles have efficiencies that are higher than the reference data at the same TITs, although the cycle boundary conditions are not identical.

- The distinct differences in the organic fluids show limited effects on the performance of the combined cycle. This is true, especially for large-scale sCO$_2$-ORC-combined cycles [50]. In the literature, both pure substances and zeotropic mixtures [43,59,60] were investigated. The nature of organic fluids decides the efficiency improvement that rises with TIT, like R245fa [42] and Isopentane [44], or falls, like the isobutane and the n-butane/isopentane mixture [43], as shown in Figure 7.

One drawback of the ORC cycle is the pinch problem or constant temperature evaporation in the evaporator. Alternatively, the tCO$_2$ cycle and Kalina cycle are potentially

useful technologies when applied to low-temperature heat sources. CO_2 is an ideal choice as the working fluid for transcritical operations due to its high performance, compactness, and non-flammability. Additionally, it is cost-effective, exhibits low toxicity, and has a negligible environmental impact. The transcritical process makes the tCO_2 cycle absorb heat at the gliding temperature instead of at the constant temperature evaporation in subcritical conditions. There are two objectives for the tCO_2 cycle, which are additional to the sCO_2 cycle.

- For power generation, Yari and Sirousazar [41] first added a tCO_2 cycle to the recompression sCO_2 cycle, showing an efficiency improvement of around 5.1%. They also showed that the performance of the combined cycle was independent of TIT but was strongly affected by the ambient temperature. When increasing the ambient temperature from 15 °C to 25 °C, the gain in efficiency went down from 5.1% to 2.7%. Alsagri and Chiasson [58] reported that the recompression cycle using a split-flow tCO_2 bottoming cycle obtained 2% more efficiency than that with a non-recuperated tCO_2 cycle. As can be seen in Figure 7, the recuperated sCO_2 cycle, for which the heat source is a molten carbonate fuel cell, was improved by 4.8–6.5% in terms of efficiency, depending on the recuperator effectiveness at a CIT of 55 °C [45,46]. When the CIT was lowered to 32 °C, the gain in efficiency for the tCO_2 cycle was up to 7.2% [2].
- For cold production, Akbari and Mahmoudi [54] proposed a recompression sCO_2 cycle combining a tCO_2 refrigeration cycle for both power and refrigeration production. In the combined cycle, a fraction of CO_2 leaving the cooler expends in the refrigeration cycle; after being heated and compressed, it then goes back to the cooler. They showed that the combined cycle produced 240 MW of power and 60 MW of cold simultaneously, or 562 MW of cold only. Manjunath et al. [61] studied a similar combined cycle utilizing the shipboard gas turbine exhaust. The proposed cycle generated a net power output of 3.0 MW (about 14.5% engine power) and a cooling output of 3.1 MW (about 15% engine power).

Although interesting studies have been published on the exergoeconomic performance of the combined sCO_2 cycle, as shown in Table 2, the techno-economic evaluation is still uncertain due to the lack of experimental facilities and standard equipment. Want et al. [23] conducted the thermoeconomic analysis of a combined recompression sCO_2-tCO_2 cycle, showing that the capital cost per net power output was about 6% more expensive than that of the stand-alone sCO_2 cycle. The heat exchanger accounted for 53% of the total cost. Their cost estimation was based on the equipment used in the chemical process. Later, Wang [2] showed that the recompression sCO_2 cycle with a tCO_2 cycle was 5.3% more expensive than the stand-alone cycle using modified cost functions.

The Kalina cycle uses an ammonia/water solution as the working fluid for power generation. The boiling point of the ammonia/water mixture can be adjusted to suit the heat input temperature by the appropriate choice of the mass ratio. As shown in Figure 7, the Kalina cycle improves the recompression sCO_2 cycle by 3.2–4% in terms of efficiency when compared to the sCO_2 cycle in isolation, according to the ammonia concentration in the solution [51,52]. Note that the Kalina cycle itself is much more complicated and hard to operate, which alone and with any additional cost may offset the benefit.

4. CO_2 Mixture

The modification of the thermal–physical properties of the working fluid by adding a small amount of other gases is not uncommon to improve a power cycle. As for the helium Brayton cycle, the use of a He/Xe or He/N_2 binary mixture was successful in reducing the stages of the turbomachinery due to the increment in the molecular weight of the gas mixture [71,72]. For the ORC, zeotropic mixtures have a non-isothermal phase change during evaporation and condensation, which reduces temperature mismatching and exergy destruction [73–77]. In previous studies, CO_2 mixtures were considerably investigated in refrigeration and heat pump systems [78–80], as was the transcritical Rankine cycle (TRC) for low-to-medium temperature applications [81–84].

As for the sCO_2 cycle, the critical point of CO_2 plays a crucial role in the lowest operating boundary and reduction of compression work. The adjustment of the critical point changes the cycle temperature and pressure ranges, providing the possibility of using high-temperature heat sinks. The direction and range of the critical point variation of CO_2 depend on the mixed component and its amount. In this regard, research on CO_2−based mixtures has been performed for various purposes. In 2011, the Sandia National Laboratories (SNL) [85] investigated the effect of secondary gas additions, i.e., SF_6, neon, n-butane, and methane, on the performance of a 50 kW full-scale CO_2 compressor. The Korea Advanced Institute of Science and Technology (KAIST) [18,86–88] studied the SFR using the sCO_2 cycle and first proposed the modification of the CO_2 critical point by mixing gases. Several potential gases were selected to consider their thermal stability, property database, and chemical stability in the temperature range of interest. Their goal was to shift the critical point of the pure CO_2 and, thus, expand the operating range of the cycle. The Czech Technical University (CTU) in Prague focused on the effect of gaseous admixtures on the pinch point [89] and cycle performance [90,91]. Both binary and multicomponent mixtures were considered.

Table 3 surveys gas additives in terms of the sCO_2 cycles, boundary conditions, applications, and thermal efficiencies declared in the original papers. For the Brayton cycles, including the basic, recuperated, recompression, precompression, and split expansion layouts, the CIT is always fixed at 1 °C above the critical temperature, and the TIP is fixed at a certain value. For TRC, the maximum power output is the focus of the purpose of WHR. As can be seen, although most articles considered the recompression cycle with a TIT of 550 °C, large discrepancies in thermal efficiencies were obtained from one paper to another.

Figure 8 plots the declared thermal efficiencies of the supercritical CO_2 mixture for both Brayton and Rankinecycles, as listed in Table 3. There are over 250 data, showing a wide range of cycle efficiencies. As can be seen, most Brayton cycles exhibit efficiencies in the range of 40% to 50%, and for the Rankine cycle, the efficiencies are from 6% to 10%. With low turbomachinery efficiency, the compound cycles have efficiencies of 25–32.5% [89,90]. The Brayton cycles without the recuperator have efficiencies well below 15% [88]. The wide dispersion of efficiencies is due to the cycle layout, as well as boundary conditions, such as TIT, turbomachinery efficiency, the effectiveness of heat exchangers, cooling conditions, and gas additives. Figure 8 also presents the efficiencies against TIT for all the cycles considered. In order to establish a convincing comparison, the commonly used efficiencies of the sCO_2 cycle were plotted as the reference [9]. In general, the recompression layout of the supercritical CO_2 mixture cycles outperforms other layouts and achieves efficiencies close to or even higher than the reference ones.
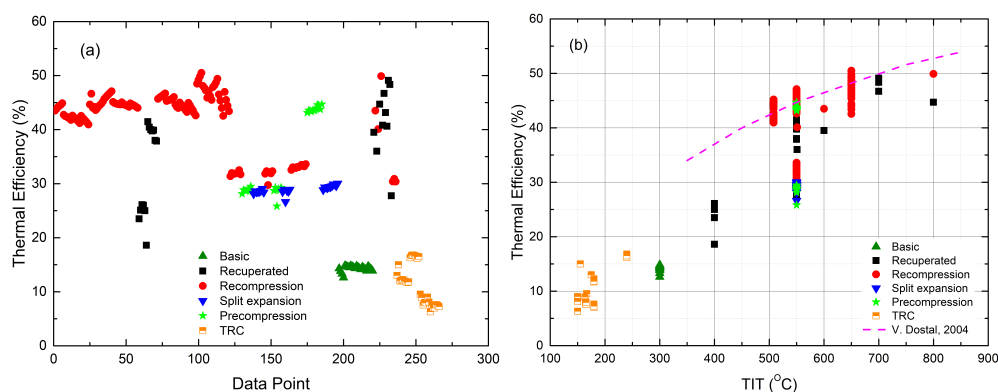
Figure 8. Thermal efficiencies of the supercritical CO_2 mixture for both Brayton and Rankinecycles considered in Table 3. (**a**) Improved thermal efficiencies. (**b**) Efficiencies as a function of TIT [9].

Table 3. Numerical study on the supercritical power cycles based on CO_2 mixture.

Cycle Layout	Initial Behavior				Improved Behavior		Application	Ref.
	CIT/°C	TIP/MPa	TIT/°C	η/%	Additives	η/%		
Recompression	32	20	508	43.27	He, Ar, N$_2$, O$_2$	41–45.2	1529 MWth Nuclear power	2011 [92]
Full-scale compressor test	27–50	-	-	-	SF$_6$, n-Butane, Neon	-	50 kW Compressor	2011 [85]
Recompression	32	20	550	45.37	He, Ar, N$_2$, O$_2$	44.02–47.1	600 MWth Nuclear power	2011 [87]
Recompression	32	20	550	45.37	Xe, Ar, N$_2$, O$_2$	44.02–46.65	600 MWth nuclear power	2011 [86]
Recuperated	40	30	400	21.5	Benzene	23.5–26.1	Not specified	2012 [93]
Recuperated	32	20	550	39.77	Xe, Kr, Ar, N$_2$, O$_2$	39.75–41.46	600 MWth Nuclear power	2013 [18]
Recompression	32	20	550	45.37	Xe, Kr, Ar, N$_2$, O$_2$	44–46.69	600 MWth nuclear power	2013 [18]
Recuperated	44	20	550	37.97	H$_2$S, Cyclohexane	37.88, 38.01	600 MWth nuclear power	2013 [18]
Recompression	44	20	550	41.36	H$_2$S, Cyclohexane	42.61, 43.23	600 MWth nuclear power	2013 [18]
Recuperated	32	20	600	37.9	N$_2$, O$_2$, Ar, Air, He	37.3–37.6	Not specified	2014 [94]
Recompression	32	20	600	42.6	N$_2$, O$_2$, Ar, Air, He	42.4–42.5	Not specified	2014 [94]
Recompression	32	20	650	47.82	O$_2$, He, Ar, Kr	45.9–50.5	600 MWth nuclear power	2015 [95]
Recompression	52	20	650	41.1	n-Butane, Cyclohexane	42.55–43.4	600 MWth nuclear power	2015 [95]
Recompression	34	24	550	32.45	He, CO, O$_2$, N$_2$, Ar, H$_2$, CH$_4$, H$_2$S	31.39–32.49	12.5 MWe Not specified	2016 [89]
Precompression	34	24	550	29.45	He, CO, O$_2$, N$_2$, Ar, H$_2$, CH$_4$, H$_2$S	28.12–29.48	16.6 MWe Not specified	2016 [89]
Split expansion	34	24	550	29.03	He, CO, O$_2$, N$_2$, Ar, H$_2$, CH$_4$, H$_2$S	28.1–29.06	11.2 MWe Not specified	2016 [89]
Recompression	34	24	550	32.45	Air, M-I, M-II, M-H, Air-H, M-IH	29.74–32.31	12.5 MWe Not specified	2017 [90]
Precompression	34	24	550	29.45	Air, M-I, M-II, M-H, Air-H, M-IH	25.83–29.29	16.6 MWe Not specified	2017 [90]
Split expansion	34	24	550	29.03	Air, M-I, M-II, M-H, Air-H, M-IH	26.62–28.91	11.2 MWe Not specified	2017 [90]
Recompression	34	27	550	33.44	He, H$_2$, CO, O$_2$, Ar, N$_2$, CH$_4$, H$_2$S, Xe, Kr, SO$_2$	32.54–33.6	38 MWth not specified	2018 [91]
Precompression	34	27	550	44.44	He, H$_2$, CO, O$_2$, Ar, N$_2$, CH$_4$, H$_2$S, Xe, Kr, SO$_2$	43.14–44.69	38 MWth not specified	2018 [91]
Split expansion	34	27	550	29.83	He, H$_2$, CO, O$_2$, Ar, N$_2$, CH$_4$, H$_2$S, Xe, Kr, SO$_2$	28.83–30.03	38 MWth not specified	2018 [91]
Basic	40	20	300	13.15	SF$_6$, R32, R22, R123, R134a, Toluene	13.86–14.49	1 MWth not specified	2018 [88]
Recuperated	40	25	551	31.3	TiCl$_4$	36	CSP	2018 [96]
Recuperated	40	25	800	40.7	TiCl$_4$	44.7	CSP	2018 [96]
Recompression	40	25	551	38.4	TiCl$_4$	40.1	CSP	2018 [96]
Recompression	40	25	800	47	TiCl$_4$	49.9	CSP	2018 [96]
Recuperated	51	25	550, 700	40.4, 47.4	N$_2$O$_4$	40.8, 46.7	100 MWth CSP	2019 [97]
Recuperated	51	25	550, 700	40.44, 47.4	N$_2$O$_4$, TiCl$_4$	40.63–49.11	33–38 MWe CSP	2019 [98]
Recuperated, recompression, partial cooling	36	25	550	27.5–30.6	Xe, n-Butane	27.7–30.9	1 MWe CSP	2019 [99]
TRC	15	10, 12	175, 155	-	SF$_6$	13, 15	Geothermal water	2013 [100]
TRC	25	10	120–240	6.8–15.6	R32, R1270, R161, R1234yf, R134a, R152a, R1234ze	7.5–16.85	20–45 kWe WHR	2014 [81]
TRC	23	11–17	170	8.97	R32, R161, R290, R1234yf, R1234ze	7.54–9.54	112 kWe WHR	2017 [82]
TRC	20	-	150	6.6	R152a, R161, R290, R1270, R1234yf, R1234ze	6.3–9	223 kWe geothermal water	2017 [101]
TRC	20	-	180	5.79	Propane, n-Butane, isobutane, n-pentane, iso-pentane, neo-pentane	7.25–7.61	20 kWe Not specified	2017 [102]
TRC	26	9	277	6.55	R290, R152a, R41, R32, R134a, R161, R1234yf, R1234ze	8.7–11.5	13 kWe WHR	2018 [83]
TRC	30	-	200	-	R134a, R32, R152a, R41, R161, R1270, R1234ze(E), R1234yf	-	20–60 kWe WHR	2018 [84]

Figure 9 plots the influence of additives on cycle thermal efficiency. The efficiency change is defined as the thermal efficiency difference between the CO_2 mixture cycle and the pure CO_2 cycle. As can be seen, some additives do not improve cycle efficiency as might be anticipated, which are Ar, N_2, O_2 [86,87], CO, CH_4, and H_2 [89,91]. These additives alone with He, Xe [86,87], and Kr [18,91] decrease the critical temperature of CO_2. However, the Xe and Kr additives improve the Brayton cycle by up to 2% in terms of efficiency, depending on the mass fraction. It was found that simultaneously lowering the critical temperature and critical pressure of the CO_2 mixture has a positive effect on the total cycle efficiency. The decrease in critical pressure leads to an increase in the cycle operating pressure ratio. It is interesting that the addition of small amounts of Kr leads to an increase and then a decrease in the critical pressure. The reported difference in cycle efficiency was down to -0.7% for the CO_2/Kr binary mixture consisting of 1% mol impurities when compared to pure CO_2 [91]. For the CO_2/He mixture, Jeong et al. [18] and Hu et al. [95] showed positive effects, whereas Vesely et al. [89] showed detrimental effects. They all used the REFPROP program, although Jeong et al. [18] pointed out that the properties of the CO_2/He mixture were opposite to the experiment data.
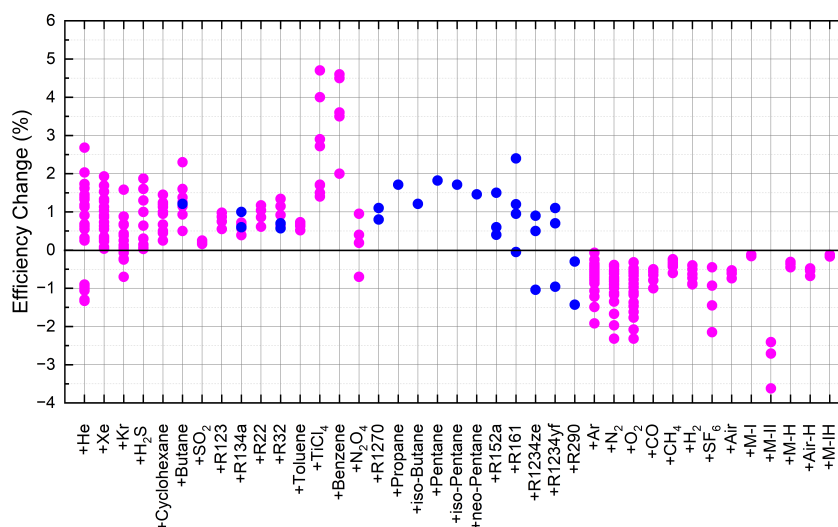
Figure 9. Changes in the thermal efficiency of the CO_2-mixture's Brayton and Rankine cycles with respect to the corresponding pure CO_2 cycles (magenta: Brayton cycle; blue: Rankine cycle).

The substances H_2S, cyclohexane, n-butane, toluene, SO_2, R123, R134a, R22, R32, and $TiCl_4$ have higher critical temperatures than pure CO_2. For these gas additives, the benefit from the compression near the critical point is maintained at high cooling conditions. As can be seen in Figure 9, adding the substances increases the cycle efficiency, ranging from 0 to 2.0%. The $CO_2/TiCl_4$ mixture makes the Brayton cycle efficiency increase in the range of 1.5% to 5%. The findings in the literature show that adding the above additives to CO_2 cannot stop cycle efficiency from decreasing in a warm environment, although the compression work is still reduced. Adding a gas to CO_2 just mitigates the extent of the efficiency reduction. At a CIT of 44 °C for a dry cooling system, the efficiency of a recompression sCO_2 cycle decreased from 45.4% to 41.4%, whereas adding H_2S and cyclohexane to the working fluid reduced the efficiency to 43.2% and 42.6%, respectively [18]. In addition, the findings show that the higher the ambient temperature, the more obvious the advantages of the method of the CO_2 mixture. A higher ambient temperature requires a higher CIT; thus, a larger amount of gas should be added. Adding $TiCl_4$ may be a better choice in a high ambient temperature situation, showing an increase in efficiency of 5.5% higher than the pure CO_2 Brayton cycle. In addition, the $CO_2/TiCl_4$ working fluid reduced the power cycle capital cost by 14.5–17.5% [98]. It is noted that several CO_2-based mixtures were tested using the sCO_2 equipment. The CO_2/n-butane, $CO_2/neon$, and CO_2/SF_6 mixtures were

tested in a full-scale compressor at SNL [85]. The performance of the CO_2/R32 mixture with mass fractions of 0.88:0.12 was tested in the compressor, showing that a slightly higher pressure ratio was achieved [88].

The investigated multicomponent mixtures are Air, M-I, M-II, M-H, Air-H, and M-IH [90]. The basic multicomponent mixture is from the technology of carbon capture and storage. The rest of the mixtures are combinations of pure additives and basic multicomponents. As can be seen in Figure 9, the multicomponent mixtures have a negative effect on the sCO_2 cycle. The effect was small if the purity of CO_2 was over 99%. If the purity of CO_2 drops under 99%, the effect of the mixture deteriorates. The cycle output could be significantly decreased by the M-II mixtures, as shown in Figure 10, which shows the thermal efficiency and power output changes of the sCO_2 cycles when the CO_2−based mixture was applied as the working fluid with respect to the original cycles.
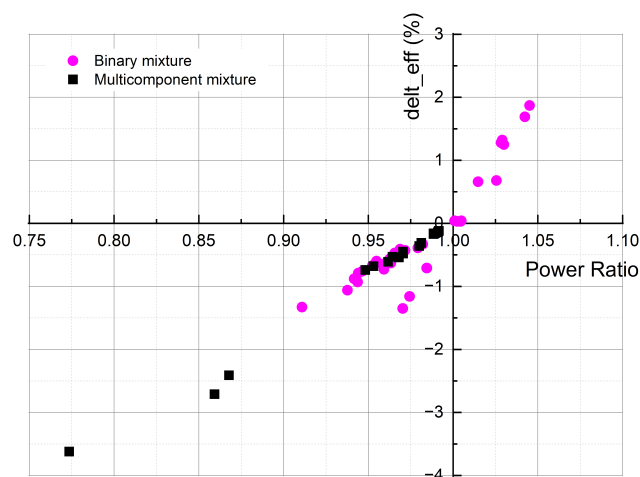
Figure 10. The efficiency and power output changes for the sCO_2 cycles with additive gases.

Mixing SF_6 with CO_2 increases the critical temperature, as calculated by the REFPROP program. However, it was found that the CO_2/SF_6 mixture for the Brayton cycle had less efficiency than the pure sCO_2 cycle at the same CIT [88]. As shown in Figure 9, the SF_6 additive reduced the cycle efficiency by 2.1% at most (with a mass fraction of 0.4). This may indicate that the critical point predicted by REFPROP is not close to the experimental value. Earlier, Lewis et al. [85] showed that the addition of SF_6 to a CO_2-dominated mixture reduced the critical temperature until SF_6 became the dominant component. A good prediction of CO_2/SF_6 mixture behavior should be further investigated.

For the Rankine cycle, the substances R1270, R161, R152a, R1234ze, R1234yf, R290, R32, and R134a were blended with CO_2, showing an efficiency gain in the range of −1.5% to 2.5%. The CO_2/R161 mixture exhibited the best cycle efficiency [81] and the most effective economic performance [82]. Note that R161 is highly flammable until the CO_2 fraction is higher than 70% [103]. The CO_2/R290 mixture is commonly used in refrigeration and heat pump systems with good performance, whereas it had decreased efficiency when used in the WHR system, as shown in Figure 9. Note that for the WHR system, the selection of the amount of additive is used to convert as much heat to power as possible; hence, the heat source temperature is not always very high.

The selection of a CO_2 mixture should simultaneously take into account thermal properties, cycle efficiency, heat transfer performance, safety, and environmental issues. To date, the choice of CO_2 mixtures has mainly considered the effect on Brayton cycle efficiency by using the basic law of thermodynamics. The thermal stability of the mixture has been less of a concern. The supercritical CO_2 mixture Brayton cycles operate at a temperature of 350 °C to 700 °C, raising the possibility of bond-breaking reactions and the further decomposition of the additive. Beyond the critical value of thermal stability, organic fluid pyrolysis yields gas, liquid, or solid products. The gaseous products (like non-condensing

gases) circulate with the working fluid, whereas the solid products stick to the surface of the heat exchanger, both of which will worsen the heat transfer. In addition, the decomposition products are mixed with the working medium, which changes the thermal properties of the working medium and makes the system deviate from the design condition, resulting in a reduction in system output power [104,105]. More seriously, molecular polymerization may occur, resulting in the blockage of a pipeline and causing a hidden danger to the system safety [106].

Table 4 collects the CO_2 mixtures that have positive effects on the power cycle mentioned above. The physical properties, safety, and environmental data are also presented. H_2S is a highly flammable and explosive gas. It was shown that its initial decomposition to hydrogen and sulfur occurred at a temperature below 444.6 °C [107,108]. The equilibrium concentration of hydrogen was less than 1% until the temperature rose up to 550 °C and about 6% at 800 °C [109]. SO_2 is chemically stable and was used as an early refrigerant in home refrigerators. Iron, steel, nickel, copper-nickel alloys, and Inconel nickel-chromium-iron are satisfactory for dry or hot SO_2 but are readily corroded by wet SO_2 gas [110]. The study of $TiCl_4$ as a heat pipe fluid in the intermediate temperature range of 400–700 K was proposed by Davarakonda and Olminsky [111], and the thermophysical properties were evaluated by NASA [112]. The experimental analysis showed that $TiCl_4$ was remarkably stable at temperatures up to 500 °C [113]. These considerations and studies support the application of $TiCl_4$ in high-temperature ORC [114]. N_2O_4 is one of the chemically reactive gases that undergo dissociation reactions at high temperatures and recombination at low temperatures. At temperatures of 30-170 °C, N_2O_4 is unstable and decomposes into NO_2, which undergoes subsequent thermal decomposition into O_2 and NO, depending on the pressure and temperature [115].

Table 4. Physical, safety, and environmental data for promising additives.

Type	Substance	Physical Data				Safety	Environmental Data [116]	
		$M/\text{g·mol}^{-1}$	P_c/MPa	$T_c/°C$	$T_D/°C$		ODP	GWP
Inorganics	H_2S	34.08	9	99.95	<444.6 [107,108]	Highly Flammable	0	-
	SO_2	64.06	7.884	157.49	2000 [110]	B1	0	-
	$TiCl_4$	189.7	4.661	364.85	>500 [113]	Non Flammable	0	-
	N_2O_4	92.01	9.976	158.2	30 [115]	Non Flammable	0	-
HC	Propane	44.10	4.251	96.74	525 [117]	Highly flammable	0	3.3
	n-Butane	58.12	3.80	152	300–320 [118]	A3	0	~20
	Pentane	72.15	3.37	196.55	280–300 [118]	A3	0	~20
	Cyclohexane	84.16	4.08	280.45	700–800 [119]	Flammable	0	20
	Benzene	78.11	4.907	288.87	<500 [120]	Highly flammable	0	20
	Toluene	92.14	4.126	318.6	350–400 [121,122]	Flammable	0	3.35
HCFC	R123	152.931	3.662	183.68	200–220 [123]	B1	0.01	77
	R125	120.02	3.6177	66.023	396 [124]	A1	0	3420
	R1270	42.08	4.66	92.4	-	A3	0	~20
	R134a	102.032	4.06	101.1	350–370 [122]	A1	0	1430
	R143a	84.04	3.761	72.71	>350 [125]	A2	0	4400
HFC	R152a	66.051	4.52	113.3	160–180 [123]	A2	0	133
	R161	48.06	5.01	102.1	427 [126]	A3	0	12
	R22	86.468	4.99	96.145	-	A1	0.055	1700
	R227ea	170.03	2.925	101.75	>425 [125]	A1	0	3300
	R236fa	152.04	3.2	124.92	380–400 [123]	A1	0	9820
	R32	52.024	5.782	78.1	570–590 [127]	A2	0	675
	R404a	97.60	3.735	72.12	-	-	0	3700
	R407c	86.20	4.632	86.2	-	A1	0	1530
	R41	34.03	5.897	44.13	-	-	0	107
	R410a	72.58	4.901	71.34	-	A1	0	1730

Organic compounds are not thermally stable at high temperatures. Between 100 °C and 500 °C, many organic molecules break down, breaking the chemical bonds in their

molecules. As can be seen in Table 4, propane, cyclohexane, benzene, R161, and R32 have relatively high decomposition temperatures. Solovyev [117] experimentally showed that propane began thermal decomposition at about 525 °C. The main products were hydrogen, methane, ethane, and ethylene. Tsang [119] proposed that the main initial processes of cyclohexane pyrolysis involved the isomerization of cyclohexane to 1-hexene, followed by the decomposition of 1-hexene. At around 800 °C, the extent of the reaction was extremely small, which is indicative of the great stability of cyclohexane. Zanetti and Egloff [120] showed that the decomposition of benzene began at temperatures as low as 500 °C. In cases below 600 °C, the amounts decomposed were small and chiefly turned into hydrogen and diphenyl at temperatures below 750 °C. As for flammability, benzene was suppressed by a volume fraction of 32% of CO_2 [128].

Several factors should also be considered when modifying the critical point of CO_2.

- The available mixture database is required. The NIST REFPROP is currently used to calculate the thermophysical properties of a CO_2 mixture. Experimental data are quite rare; only the properties of CO_2/xenon can be used so far [129]. However, the REFPROP program suggests the equation of state (EOS) temperature and pressure limits as follows: 161–750 K and 700 MPa for CO_2/Xe, 116–750 K and 200 MPa for CO_2/Kr, 188–760 K and 170 MPa for CO_2/H_2S, and 279–700 K and 80 MPa for CO_2/cyclohexane. In order to estimate the properties at higher temperatures, the temperature range of the REFPROP program has to be extended.
- The critical phenomena of CO_2 mixtures should be considered carefully. The critical line has a continuous or discontinuous form among each critical point of the pure components. As for the discontinuous critical lines, the existence of phase separation could cause instability in the CO_2 mixtures. This could hardly further obtain the optimum design of the compressor.
- The thermal stability of potential additives should be considered as a key selection criterion besides their thermodynamic performance. Otherwise, decomposition products, like non-condensable gases and deposits, may reduce the heat transfer rates, damage the components, and compromise cycle safety. Additional experiments are needed to identify the real phenomena of CO_2 mixtures at high temperatures.
- The chemical effect on cycle components should be considered in the future.

5. Strengths and Weaknesses Analysis

In order to compare the three categorized methods discussed above, the strengths and weaknesses have been identified and are listed in Table 5.

The conventional method provides a moderate enhancement to the sCO_2 cycle. A promising power cycle always comes at the cost of high cycle complexity. More components and complex control strategies would make off-design operations less flexible than the recuperated layout of the sCO_2 cycle. It was found that the recompression sCO_2 cycle is able to yield a high efficiency while still retaining simplicity.

The combined cycle could largely improve the sCO_2 cycle by recovering waste heat from the cooler. At least four more components are required, which increases the capital cost by about 5% [2,23]. The challenging task of this approach is the condensation of the working fluid in the bottoming cycle. Wet cooling or a low-temperature heat sink is mandatory, especially for the tCO_2 bottoming cycle. If the terrestrial ambient temperature is too high or if dry cooling is employed, it is difficult or even impossible to cool the working fluid sufficiently.

The CO_2 mixture method increases the thermal efficiency of the sCO_2 cycle in an economical way. The adjustment of the critical temperature and pressure of the working fluid broadens the applicability of the sCO_2 cycle for a variety of possible heat sinks. The selection of additives plays a crucial role in cycle performance, heat transfer, thermal stability, control, and chemical stability.

Table 5. Strengths and weaknesses of sCO_2 cycle improvement methods.

Method	Strengths	Weaknesses
Conventional method	• Moderate efficiency rise • Technology proven (on steam Rankine cycles)	• Adding component(s) • Complex layout • High TIT • Large pressure drop
Combined cycle	⊠ Good waste heat recovery ⊠ Large efficiency rise ⊠ Combined cold and power cogeneration	⊠ Additional components ⊠ Capital cost increase ⊠ Complex layout ⊠ Wet cooling needed
CO_2 mixture	• Low efficiency rise • Cost-effective • Applicable to hot-arid environments	• Thermal stability of additives • Control of additives • Chemical reaction with materials

6. Conclusions

This paper surveys the available methods of enhanced sCO_2 cycles and uses thermodynamics to gain insight into the effects of cycle modification. These approaches were classified into three categories by type and characteristic: the conventional method, CO_2 mixture, and combined cycle. The comparison of each method was based on the values declared in the original papers, which were investigated under very different operating conditions. An intuitive overview of the performance enhancement is provided for the sCO_2 cycle. In addition, the strengths and limitations of each method are discussed.

In general, the conventional method shows moderate efficiency improvements. Adding a bottoming cycle is a promising option that can significantly improve efficiency. The drawbacks are the requirement of a year-round supply of cold cooling water and about a 5% increase in the capital cost. The modification of the thermal–physical properties of CO_2 is an economical way to change cycle performance. The higher the ambient temperature, the more obvious the advantages of the method of critical point shifting. Thermal stability and the property database are crucial factors for gas mixture selections. Combining the potential methods is a better choice. Further steps toward a comparison of the three methods under the same operating conditions should be conducted.

Author Contributions: Conceptualization, X.W. and X.F.; methodology, J.W. and M.H.; resources, L.Z. and Z.Z.; writing—original draft preparation, L.Z. and Z.Z.; writing—review and editing, X.W. and X.F.; project administration, X.W.; funding acquisition, X.W. All authors have read and agreed to the published version of the manuscript.

Data Availability Statement: Not applicable.

Conflicts of Interest: The authors declare no conflicts of interest.

Abbreviations

The following abbreviations are used in this manuscript:

sCO_2	supercritical carbon dioxide
tCO_2	transcritical carbon dioxide
TIT	turbine inlet temperature
TIP	turbine inlet pressure
CIT	compressor inlet temperature
CSP	concentrating solar power
WHR	waste heat recovery
ORC	organic Rankine cycle

TRC	transcritical Rankine cycle
EOS	equation of state
LNG	liquefied natural gas

References

1. Brun, K.; Friedman, P.; Dennis, R. *Fundamentals and Applications of Supercritical Carbon Dioxide (sCO₂) Based Power Cycles*; Woodhead Publishing: Sawston, UK, 2017.
2. Wang, X. A Supercritical CO_2 Brayton Cycle Based Cogeneration System. Ph.D. Thesis, Xi'an Jiaotong University, Xi'an, China, 2018. (In Chinese)
3. Tollefson, J. Innovative zero-emissions power plant begins battery of tests. *Nature* **2018**, *557*, 622–623. [CrossRef] [PubMed]
4. Southwest Research Institute. *SwRI, GTI and GE Break Ground on $119 Million Supercritical CO_2 Pilot Power Plant*. Available online: https://www.swri.org/press-release/swri-gti-ge-supercritical-CO2-pilot-power-plant (accessed on 18 September 2023).
5. Benra, F.; Brillert, D.; Frybort, O.; Hajek, P.; Rohde, M.; Schuster, S.; Seewald, M.; Starflinger, J. A supercritical CO_2 low temperature Brayton cycle for residual heat removal. In Proceedings of the 5th International Symposium—Supercritical CO_2 Power Cycles, San Antonio, TX, USA, 8–31 March 2016.
6. Institute of Engineering Thermophysics. China's First Large-Scale Supercritical Carbon Dioxide Compressor Experimental Platform Completed and Put Into Operation. Available online: http://www.bjb.cas.cn/kjdt2016/201809/t20180929\protect\relax$\@@underline{\hbox{}}\mathsurround\z@$\relax5110326.html (accessed on 18 September 2023). (In Chinese)
7. Institute of Engineering Thermophysics. Construction of a Comprehensive Test Platform for Full-Temperature Full-Pressure Supercritical Carbon Dioxide Heat Exchanger. Available online: http://www.dnl.ac.cn/info/1025/1167.htm (accessed on 18 September 2023). (In Chinese)
8. Singh, R. Dynamics and Control of a Closed Carbon-Dioxide Brayton Cycle. Ph.D. Thesis, The University of Queensland, Brisbane, Australia, 2013.
9. Dostal, V. A Supercritical Carbon Dioxide Cycle for Next Generation Nuclear Reactors. Ph.D. Thesis, Massachusetts Institute of Technology, Cambridge, MA, USA, 2004.
10. Dyreby, J.J. Modeling the Supercritical Carbon Dioxide Brayton Cycle with Recompression. Ph.D. Thesis, University of Wisconsin-Madison, Madison, WI, USA, 2014.
11. de la Calle, A.; Bayon, A.; Too, Y.C.S. Impact of ambient temperature on supercritical CO_2 recompression Brayton cycle in arid locations: Finding the optimal design conditions. *Energy* **2018**, *153*, 1016–1027. [CrossRef]
12. Moisseytsev, A.; Sienicki, J. *Performance Improvement Options for the Supercritical Carbon Dioxide Brayton Cycle*; Technical Report; ANL-GenIV-103; Argonne National Laboratory: Argonne, IL, USA, 2007.
13. Ahn, Y.; Bae, S.J.; Kim, M.; Cho, S.K.; Baik, S.; Lee, J.I.; Cha, J.E. Review of supercritical CO_2 power cycle technology and current status of research and development. *Nucl. Eng. Technol.* **2015**, *47*, 647–661. [CrossRef]
14. Crespi, F.; Gavagnin, G.; Sánchez, D.; Martínez, G.S. Supercritical Carbon Dioxide Cycles for Power Generation: A Review. *Appl. Energy* **2017**, *195*, 152–183. [CrossRef]
15. Li, M.; Zhu, H.; Guo, J.; Wang, K.; Tao, W. The development technology and applications of supercritical CO_2 power cycle in nuclear energy, solar energy and other energy industries. *Appl. Therm. Eng.* **2017**, *126*, 255–275. [CrossRef]
16. Wang, K.; He, Y.L.; Zhu, H.H. Integration between supercritical CO_2 Brayton cycles and molten salt solar power towers: A review and a comprehensive comparison of different cycle layouts. *Appl. Energy* **2017**, *195*, 819–836. [CrossRef]
17. Xu, J.; Liu, C.; Sun, E.; Xie, J.; Li, M.; Yang, Y.; Liu, J. Perspective of S-CO₂ power cycles. *Energy* **2019**, *186*, 115831. [CrossRef]
18. Jeong, W.S.; Jeong, Y.H. Performance of Supercritical Brayton Cycle Using CO_2−based Binary Mixture at Varying Critical Points for SFR Applications. *Nucl. Eng. Des.* **2013**, *262*, 12–20. [CrossRef]
19. Angelino, G. Real Gas Effects in Carbon Dioxide Cycles. In Proceedings of the ASME 1969 Gas Turbine Conference and Products Show, Cleveland, OH, USA, 10–13 March 1969.
20. Kato, Y.; Nitawaki, T.; Muto, Y. Medium Temperature Carbon Dioxide Gas Turbine Reactor. *Nucl. Eng. Des.* **2004**, *230*, 195–207. [CrossRef]
21. Ma, Y.; Liu, M.; Yan, J.; Liu, J. Thermodynamic Study of Main Compression Intercooling Effects on Supercritical CO_2 Recompression Brayton Cycle. *Energy* **2017**, *140*, 746–756. [CrossRef]
22. Couso, G.B.; Vicencio, R.B.; Padilla, R.V.; Too, Y.C.S.; Pye, J. Dynamic Model of Supercritical CO_2 Brayton Cycles Driven by Concentrated Solar Power. In Proceedings of the ASME 2017 11th International Conference on Energy Sustainability, American Society of Mechanical Engineers, Charlotte, NC, USA, 26–30 June 2017; p. V001T05A008.
23. Wang, X.; Wu, Y.; Wang, J.; Dai, Y.; Xie, D. Thermo-economic Analysis of A Recompression Supercritical CO_2 Cycle Combined With A Transcritical CO_2 Cycle. In Proceedings of the ASME Turbo Expo 2015: Turbine Technical Conference and Exposition, Montréal, QC, Canada, 15–19 June 2015.
24. Stamatellos, G.; Stamatelos, T. Effect of actual recuperators effectiveness on the attainable efficiency of supercritical CO_2 Brayton cycles for solar thermal power plants. *Energies* **2022**, *15*, 7773. [CrossRef]
25. Ren, Z.; Zhao, C.R.; Jiang, P.X.; Bo, H.L. Investigation on local convection heat transfer of supercritical CO_2 during cooling in horizontal semicircular channels of printed circuit heat exchanger. *Appl. Therm. Eng.* **2019**, *157*, 113697. [CrossRef]

26. Stamatellos, G.; Stamatellou, A.; Kalfas, A.I. CFD —Aided design methodology for PCHE-type recuperators in supercritical CO_2 recompression power cycles. In Proceedings of the ASME Turbo Expo 2020: Turbomachinery Technical Conference and Exposition, New York, NY, USA, 21–25 September 2020.

27. Dostal, V.; Driscoll, M.J.; Hejzlar, P.; Todreas, N.E. A Supercritical CO_2 Gas Turbine Power Cycle for Next-generation Nuclear Reactors. In Proceedings of the 10th International Conference on Nuclear Engineering, Arlington, VA, USA, 14–18 April 2002.

28. Sarkar, J.; Bhattacharyya, S. Optimization of Recompression S-CO_2 Power Cycle With Reheating. *Energy Convers. Manag.* **2009**, *50*, 1939–1945. [CrossRef]

29. Kulhanek, M.; Dostal, V. Thermodynamic Analysis and Comparison of Supercritical Carbon Dioxide Cycles. In Proceedings of the Supercritical CO_2 Power Cycle Symposium, Boulder, CO, USA, 24–25 May 2011.

30. Turchi, C.S.; Ma, Z.; Neises, T.; Wagner, M. Thermodynamic Study of Advanced Supercritical Carbon Dioxide Power Cycles for High Performance Concentrating Solar Power Systems. In Proceedings of the ASME 2012 6th International Conference on Energy Sustainability, San Diego, CA, USA, 23–26 July 2012.

31. Turchi, C.S.; Ma, Z.; Dyreby, J. Supercritical Carbon Dioxide Power Cycle Configuration for Use in Concentrating Solar Power Systems. In Proceedings of the ASME Turbo Expo 2012: Turbine Technical Conference and Exposition, American Society of Mechanical Engineers, Copenhagen, Denmark, 11–15 June 2012; pp. 967–973.

32. Padilla, R.V.; Benito, R.G.; Stein, W. An Exergy Analysis of Recompression Supercritical CO_2 Cycles With and Without Reheating. *Energy Procedia* **2015**, *69*, 1181–1191. [CrossRef]

33. Padilla, R.V.; Too, Y.C.S.; Beath, A.; McNaughton, R.; Stein, W. Effect of Pressure Drop and Reheating on Thermal and Exergetic Performance of Supercritical Carbon Dioxide Brayton Cycles Integrated With a Solar Central Receiver. *J. Sol. Energy Eng.* **2015**, *137*, 051012. [CrossRef]

34. Mounir Mecheri, Y.L.M. Supercritical CO_2 Brayton Cycles for Coal-fired Power Plants. *Energy* **2016**, *103*, 758–771. [CrossRef]

35. Purjam, M.; Goudarzi, K.; Keshtgar, M. A New Supercritical Carbon Dioxide Brayton Cycle with High Efficiency. *Heat Transf.—Asian Res.* **2017**, *46*, 465–482. [CrossRef]

36. Coco-Enriquez, L.; Munoz-Anton, J.; Martinez-Val, J. Thermodynamic Optimization of Supercritical CO_2 Brayton Power Cycles Coupled to Line-Focusing Solar Fields. *J. Sol. Energy Eng.* **2017**, *139*, 061005. [CrossRef]

37. Binotti, M.; Astolfi, M.; Campanari, S.; Manzolini, G.; Silva, P. Preliminary Assessment of sCO2 Cycles for Power Generation in CSP Solar Tower Plants. *Appl. Energy* **2017**, *204*, 1007–1017. [CrossRef]

38. Coco-Enriquez, L.; Munoz-Anton, J.; Martinez-Val, J. Dual Loop Line-Focusing Solar Power Plants With Supercritical Brayton Power Cycles. *Int. J. Hydrogen Energy* **2017**, *42*, 17664–17680. [CrossRef]

39. Moisseytsev, A. Passive Load Follow Analysis of the STAR-LM and STAR-H_2 Systems. Ph.D. Thesis, Texas A&M University, College Station, TX, USA, 2003.

40. Angelino, G. Carbon Dioxide Condensation Cycles for Power Production. *J. Eng. Power Trans. ASME* **1968**, *90*, 287–295. [CrossRef]

41. Yari, M.; Sirousazar, M. A Novel Recompression S-CO_2 Brayton Cycle With Pre-cooler Exergy Utilization. *Proc. Inst. Mech. Eng. Part A J. Power Energy* **2010**, *224*, 931–946. [CrossRef]

42. Chacartegui, R.; de Escalona, J.M.; Sánchez, D.; Monje, B.; Sánchez, T. Alternative Cycles Based on Carbon Dioxide for Central Receiver Solar Power Plants. *Appl. Therm. Eng.* **2011**, *31*, 872–879. [CrossRef]

43. Sánchez, D.; Brenes, B.M.; de Escalona, J.M.M.; Chacartegui, R. Non-conventional Combined Cycle for Intermediate Temperature Systems. *Int. J. Energy Res.* **2013**, *37*, 403–411. [CrossRef]

44. Besarati, S.M.; Goswami, D.Y. Analysis of Advanced Supercritical Carbon Dioxide Power Cycles With a Bottoming Cycle for Concentrating Solar Power Applications. *J. Sol. Energy Eng.* **2014**, *136*, 010904. [CrossRef]

45. Bae, S.J.; Ahn, Y.; Lee, J.; Lee, J.I. Hybrid System of Supercritical Carbon Dioxide Brayton Cycle and Carbon Dioxide Rankine Cycle Combined Fuel Cell. In Proceedings of the ASME Turbo Expo, Düsseldorf, Germany, 16–20 June 2014.

46. Bae, S.J.; Ahn, Y.; Lee, J.; Lee, J.I. Various Supercritical Carbon Dioxide Cycle Layouts Study for Molten Carbonate Fuel Cell Application. *J. Power Sources* **2014**, *270*, 608–618. [CrossRef]

47. Zhang, H.; Shao, S.; Zhao, H.; Feng, Z. Thermodynamic Analysis of a SCO2 Part-Flow Cycle Combined With an Organic Rankine Cycle With Liquefied Natural Gas as Heat Sink. In Proceedings of the ASME Turbo Expo 2014: Turbine Technical Conference and Exposition, American Society of Mechanical Engineers, Düsseldorf, Germany, 16–20 June 2014; p. V03BT36A012.

48. Akbari, A.D.; Mahmoudi, S.M. Thermoeconomic Analysis & Optimization of the Combined Supercritical CO_2 (Carbon Dioxide) Recompression Brayton/Organic Rankine Cycle. *Energy* **2014**, *78*, 501–512.

49. Wang, X.; Wang, J.; Zhao, P.; Dai, Y. Thermodynamic comparison and optimization of supercritical CO_2 Brayton cycles with a bottoming transcritical CO_2 cycle. *J. Energy Eng.* **2015**, *142*, 04015028. [CrossRef]

50. Wang, X.; Dai, Y. Exergoeconomic Analysis of Utilizing the Transcritical CO_2 Cycle and the ORC for A Recompression Supercritical CO_2 Cycle Waste Heat Recovery: A Comparative Study. *Appl. Energy* **2016**, *170*, 193–207. [CrossRef]

51. S Mahmoudi, S.M.; D Akbari, A.; Rosen, M.A. Thermoeconomic Analysis and Optimization of A New Combined Supercritical Carbon Dioxide Recompression Brayton/Kalina cycle. *Sustainability* **2016**, *8*, 1079. [CrossRef]

52. Li, H.; Wang, M.; Wang, J.; Dai, Y. Exergoeconomic Analysis and Optimization of A Supercritical CO_2 Cycle Coupled With A Kalina Cycle. *J. Energy Eng.* **2016**, *143*, 04016055. [CrossRef]

53. Mahmoudi, S.; Ghavimi, A. Thermoeconomic analysis and multi objective optimization of a molten carbonate fuel cell—Supercritical carbon dioxide—Organic Rankin cycle integrated power system using liquefied natural gas as heat sink. *Appl. Therm. Eng.* **2016**, *107*, 1219–1232. [CrossRef]

54. Akbari, A.; Mahmoudi, S. Thermoeconomic Performance and Optimization of A Novel Cogeneration System Using Carbon Dioxide as Working Fluid. *Energy Convers. Manag.* **2017**, *145*, 265–277. [CrossRef]

55. Cao, Y.; Ren, J.; Sang, Y.; Dai, Y. Thermodynamic analysis and optimization of a gas turbine and cascade CO_2 combined cycle. *Energy Convers. Manag.* **2017**, *144*, 193–204. [CrossRef]

56. Hou, S.; Wu, Y.; Zhou, Y.; Yu, L. Performance analysis of the combined supercritical CO_2 recompression and regenerative cycle used in waste heat recovery of marine gas turbine. *Energy Convers. Manag.* **2017**, *151*, 73–85. [CrossRef]

57. Wang, X.; Yang, Y.; Zheng, Y.; Dai, Y. Exergy and exergoeconomic analyses of a supercritical CO_2 cycle for a cogeneration application. *Energy* **2017**, *119*, 971–982. [CrossRef]

58. Alsagri, A.S.; Chiasson, A.D. Thermodynamic Analysis and Multi-Objective Optimizations of a Combined Recompression SCO_2 Brayton Cycle-TCO_2 Rankine Cycles for Waste Heat Recovery. *Int. J. Curr. Eng. Technol.* **2018**, *8*, 541–548.

59. Hou, S.; Cao, S.; Yu, L.; Zhou, Y.; Wu, Y.; Zhang, F. Performance Optimization of Combined Supercritical CO_2 Recompression Cycle and Regenerative Organic Rankine Cycle Using Zeotropic Mixture Fluid. *Energy Convers. Manag.* **2018**, *166*, 187–200. [CrossRef]

60. Hou, S.; Zhou, Y.; Yu, L.; Zhang, F.; Cao, S.; Wu, Y. Optimization of A Novel Cogeneration System Including A Gas Turbine, A Supercritical CO_2 Recompression Cycle, A Steam Power Cycle and An Organic Rankine Cycle. *Energy Convers. Manag.* **2018**, *172*, 457–471. [CrossRef]

61. Manjunath, K.; Sharma, O.; Tyagi, S.; Kaushik, S. Thermodynamic Analysis of A Supercritical/transcritical CO_2 Based Waste Heat Recovery Cycle for Shipboard Power and Cooling Applications. *Energy Convers. Manag.* **2018**, *155*, 262–275. [CrossRef]

62. Singh, H.; Mishra, R. Performance Analysis of Solar Parabolic Trough Collectors Driven Combined Supercritical CO_2 and Organic Rankine Cycle. *Eng. Sci. Technol. Int. J.* **2018**, *21*, 451–464.

63. Song, J.; song Li, X.; dong Ren, X.; wei Gu, C. Performance Analysis and Parametric Optimization of Supercritical Carbon Dioxide (S-CO_2) Cycle With Bottoming Organic Rankine Cycle (ORC). *Energy* **2018**, *143*, 406–416. [CrossRef]

64. Cao, Y.; Rattner, A.S.; Dai, Y. Thermoeconomic analysis of a gas turbine and cascaded CO_2 combined cycle using thermal oil as an intermediate heat-transfer fluid. *Energy* **2018**, *162*, 1253–1268. [CrossRef]

65. Dipippo, R. *Geothermal Power Plants. Principles Applications, and Case Studies*; Elsevier Science: Amsterdam, The Netherlands, 2005.

66. Harinck, J.; Turunen-Saaresti, T.; Colonna, P.; Rebay, S.; van Buijtenen, J. Computational Study of A High Expansion Ratio Radial Organic Rankine Cycle Turbine Stator. *J. Eng. Gas Turbines Power* **1996**, *118*, 359–367. [CrossRef]

67. Drescher, U.; Bruggemann, D. Fluid Selection for the Organic Rankine Cycle (ORC) in Biomass Power and Heat Plants. *Appl. Therm. Eng.* **2007**, *27*, 223–228. [CrossRef]

68. Lai, N.A.; Wendland, M.; Fischer, J. Working Fluids for High-Temperature Organic Rankine Cycles. *Energy* **2011**, *36*, 199–211. [CrossRef]

69. Quoilin, S.; Aumann, R.; Grill, A.; Schuster, A.; Lemort, V.; Spliethoff, H. Dynamic Modeling and Optimal Control Strategy of Waste Heat Recovery Organic Rankine Cycles. *Appl. Energy* **2011**, *88*, 2183–2190. [CrossRef]

70. Chacartegui, R.; Sánchez, D.; Jiménez-Espadafor, F.; Muñoz, A.; Sánchez, T. Analysis of Intermediate Temperature Combined Cycles With A Carbon Dioxide Topping Cycle. In Proceedings of the ASME Turbo Expo 2008: Power for Land, Sea and Air, Berlin, Germany, 9–13 June 2008; pp. 673–680.

71. El-Genk, M.; Tournier, J. Noble Gas Mixtures for Gas-cooled Reactor Power Plants. *Nucl. Eng. Des.* **2008**, *238*, 1353–1372. [CrossRef]

72. El-Genk, M.; Tournier, J. Performance Analyses of VHTR Plants With Direct and Indirect Closed Brayton Cycles and Different Working Fluids. *Prog. Nucl. Energy* **2009**, *51*, 556–572. [CrossRef]

73. Wang, X.; Zhao, L. Analysis of zeotropic mixtures used in low-temperature solar Rankine cycles for power generation. *Sol. Energy* **2009**, *83*, 605–613. [CrossRef]

74. Bao, J.; Zhao, L. A review of working fluid and expander selections for organic Rankine cycle. *Renew. Sustain. Energy Rev.* **2013**, *24*, 325–342. [CrossRef]

75. Feng, Y.; Hung, T.; Zhang, Y.; Li, B.; Yang, J.; Shi, Y. Performance comparison of low-grade ORCs (organic Rankine cycles) using R245fa, pentane and their mixtures based on the thermoeconomic multi-objective optimization and decision makings. *Energy* **2015**, *93*, 2018–2029. [CrossRef]

76. Sadeghi, M.; Nemati, A.; ghavimi, A.; Yari, M. Thermodynamic analysis and multi-objective optimization of various ORC (organic Rankine cycle) configurations using zeotropic mixtures. *Energy* **2016**, *109*, 791–802. [CrossRef]

77. Modi, A.; Haglind, F. A review of recent research on the use of zeotropic mixtures in power generation systems. *Energy Convers. Manag.* **2017**, *138*, 603–626. [CrossRef]

78. Dai, B.; Dang, C.; Li, M.; Tian, H.; Ma, Y. Thermodynamic performance assessment of carbon dioxide blends with low-global warming potential (GWP) working fluids for a heat pump water heater. *Int. J. Refrig.* **2015**, *56*, 1192145. [CrossRef]

79. Wang, D.; Lu, Y.; Tao, L. Thermodynamic analysis of CO_2 blends with R41 as an azeotropy refrigerant applied in small refrigerated cabinet and heat pump water heater. *Appl. Therm. Eng.* **2017**, *125*, 1490–1500. [CrossRef]

80. Hu, J.; Liu, C.; Li, Q.; Shi, X. Molecular simulation of thermal energy storage of mixed CO_2/IRMOF-1 nanoparticle nanofluid. *Int. J. Heat Mass Transf.* **2018**, *125*, 1345–1348. [CrossRef]

81. Dai, B.; Li, M.; Ma, Y. Thermodynamic analysis of carbon dioxide blends with low GWP (global warming potential) working fluids-based transcritical Rankine cycles for low-grade heat energy recovery. *Energy* **2014**, *64*, 942–952. [CrossRef]

82. Yang, M.H. The performance analysis of the transcritical Rankine cycle using carbon dioxide mixtures as the working fluids for waste heat recovery. *Energy Convers. Manag.* **2017**, *151*, 86 – 97. [CrossRef]

83. Shu, G.; Yu, Z.; Tian, H.; Liu, P.; Xu, Z. Potential of the transcritical Rankine cycle using CO_2-based binary zeotropic mixtures for engine's waste heat recovery. *Energy Convers. Manag.* **2018**, *174*, 668–685. [CrossRef]

84. Sánchez, C.J.; da Silva, A.K. Technical and environmental analysis of transcritical Rankine cycles operating with numerous CO_2 mixtures. *Energy* **2018**, *142*, 180–190. [CrossRef]

85. Lewis, T.; Wright, S.; Conboy, T. Supercritical CO_2 Mixture Behavior for Advanced Power Cycles and Applications. In Proceedings of the Supercritical CO_2 Power Cycle Symposium, Boulder, CO, USA, 24–25 May 2011.

86. Jeong, W.S.; Jeong, Y.H.; Lee, J.I. Performance of S-CO_2 Brayton Cycle with Additive Gases for SFR Application. In Proceedings of the Supercritical CO_2 Power Cycle Symposium, Boulder, CO, USA, 24–25 May 2011.

87. Jeong, W.S.; Lee, J.I.; Jeong, Y.H. Potential Improvements of Supercritical Recompression CO_2 Brayton Cycle by Mixing Other Gases for Power Conversion System of A SFR. *Nucl. Eng. Des.* **2011**, *241*, 2128–2137. [CrossRef]

88. Baik, S.; Lee, J.I. Preliminary Study of Supercritical CO_2 Mixed With Gases for Power Cycle in Warm Environments. In Proceedings of the ASME Turbo Expo 2018: Turbomachinery Technical Conference and Exposition, Oslo, Norway, 11–15 June 2018; p. V009T38A017.

89. Vesely, L.; Dostal, V.; Stepanek, J. Effect of Gaseous Admixtures on Cycles with Supercritical Carbon Dioxide. In Proceedings of the ASME Turbo Expo 2016: Turbomachinery Technical Conference and Exposition, GT2016, Seoul, Republic of Korea, 13–17 June 2016.

90. Vesely, L.; Dostal, V. Effect of Multicomponent Mixtures on Cycles with Supercritical Carbon Dioxide. In Proceedings of the ASME Turbo Expo 2017: Turbomachinery Technical Conference and Exposition, GT2017, Charlotte, NC, USA, 26–30 June 2017.

91. Vesely, L.; Manikantachari, K.R.V.; Vasu, S.; Kapat, J.; Dostal, V.; Martin, S. Effect of Mixtures on Compressor and Cooler in Supercritical Carbon Dioxide Cycles. In Proceedings of the ASME Turbo Expo 2018: Turbomachinery Technical Conference and Exposition, GT2018, Oslo, Norway, 11–15 June 2018.

92. Jeong, W.S.; Lee, J.I.; Jeong, Y.H.; NO, H.C. Potential Improvements of Supercritical Recompression CO_2 Brayton Cycle Coupled with KALIMER-600 by Modifying Critical Point of CO_2. In Proceedings of the Transactions of the Korean Nuclear Society Autumn Meeting, Jeju, Republic of Korea, 21–22 October 2010.

93. Invernizzi, C.M.; van der Stelt, T. Supercritical and real gas Brayton cycles operating with mixtures of carbon dioxide and hydrocarbons. *Proc. Inst. Mech. Eng. Part A J. Power Energy* **2012**, *226*, 682–693. [CrossRef]

94. Vesely, L.; Dostal, V. Research on the Effect of the Pinch Point Shift in Cycles with Supercritical Carbon Dioxide. In Proceedings of the 4th International Symposium—Supercritical CO_2 Power Cycles, Pittsburgh, PA, USA, 9–10 September 2014.

95. Hu, L.; Chen, D.; Huang, Y.; Li, L.; Cao, Y.; Yuan, D.; Wang, J.; Pan, L. Investigation on the Performance of the Supercritical Brayton Cycle With CO_2-based Binary Mixture as Working Fluid for An Energy Transportation System of A Nuclear Reactor. *Energy* **2015**, *89*, 874–886. [CrossRef]

96. Bonalumi, D.; Lasala, S.; Macchi, E. CO_2-$TiCl_4$ working fluid for high-temperature heat source power cycles and solar application. *Renew. Energy* **2020**, *147*, 2842–2854. [CrossRef]

97. Binotti, M.; Invernizzi, C.M.; Iora, P.; Manzolini, G. Dinitrogen tetroxide and carbon dioxide mixtures as working fluids in solar tower plants. *Sol. Energy* **2019**, *181*, 203–213. [CrossRef]

98. Manzolini, G.; Binotti, M.; Bonalumi, D.; Invernizzi, C.; Iora, P. CO_2 mixtures as innovative working fluid in power cycles applied to solar plants. Techno-economic assessment. *Sol. Energy* **2019**, *181*, 530–544. [CrossRef]

99. Guo, J.Q.; Li, M.J.; Xu, J.L.; Yan, J.J.; Wang, K. Thermodynamic performance analysis of different supercritical Brayton cycles using CO_2-based binary mixtures in the molten salt solar power tower systems. *Energy* **2019**, *173*, 785–798. [CrossRef]

100. Yin, H.; Sabau, A.S.; Conklin, J.C.; McFarlane, J.; Qualls, A.L. Mixtures of SF_6-CO_2 as working fluids for geothermal power plants. *Appl. Energy* **2013**, *106*, 243–253. [CrossRef]

101. Wu, C.; sen Wang, S.; Jiang, X.; Li, J. Thermodynamic analysis and performance optimization of transcritical power cycles using CO_2-based binary zeotropic mixtures as working fluids for geothermal power plants. *Appl. Therm. Eng.* **2017**, *115*, 292–304. [CrossRef]

102. Feng, L.; Zheng, D.; Chen, J.; Dai, X.; Shi, L. Exploration and Analysis of CO_2 + Hydrocarbons Mixtures as Working Fluids for Trans-critical ORC. *Energy Procedia* **2017**, *129*, 145–151. [CrossRef]

103. Zabetakis, M.G. *Flammability Characteristics of Combustible Gases and Vapors*; Technical Report; Bureau of Mines: Washington, DC, USA, 1965.

104. Badr, O.; Probert, S.; O'Callaghan, P. Selecting a working fluid for a Rankine-cycle engine. *Appl. Energy* **1985**, *21*, 1–42. [CrossRef]

105. Ginosar, D.M.; Petkovic, L.M.; Guillen, D.P. Thermal Stability of Cyclopentane as an Organic Rankine Cycle Working Fluid. *Energy Fuels* **2011**, *25*, 4138–4144. [CrossRef]

106. Dai, X.; An, Q.; Shi, L. Experiment research for the thermal stability of isobutene and isopentane. *J. Eng. Thermophys.* **2013**, *34*, 1416 –1419. (In Chinese)

107. Barin, I.; Knacke, O. *Thermochemical Properties of Inorganic Substances*; Springer Berlin: Heidelberg, Germany, 1973.
108. Fukuda, K.; Dokiya, M.; Kameyama, T.; Kotera, Y. Catalytic decomposition of hydrogen sulfide. *Ind. Eng. Chem. Fundam.* **1978**, *17*, 243–248. [CrossRef]
109. Chivers, T.; Hyne, J.B.; Lau, C. The thermal decomposition of hydrogen sulfide over transition metal sulfides. *Int. J. Hydrogen Energy* **1980**, *5*, 499–506. [CrossRef]
110. Weil, E.D.; Sandler, S.R.; Gernon, M. *Kirk-Othmer Encyclopedia of Chemical Technology*; John Wiley & Sons, Inc.: New York, NY, USA, 2006; Chapter Sulfur Compounds.
111. Devarakonda, A.; Olminsky, J. An evaluation of halides and other substances as potential heat pipe fluids. In Proceedings of the 2nd International Energy Conversion Engineering Conference, Providence, RI, USA, 16–19 August 2004; p. 5575.
112. Devarakonda, A.; Anderson, W.G. Thermo-Physical Properties of Intermediate Temperature Heat Pipe Fluids. *AIP Conf. Proc.* **2005**, *746*, 179–186.
113. Invernizzi, C.; Iora, P.; Bonalumi, D.; Macchi, E.; Roberto, R.; Caldera, M. Titanium tetrachloride as novel working fluid for high temperature Rankine Cycles: Thermodynamic analysis and experimental assessment of the thermal stability. *Appl. Therm. Eng.* **2016**, *107*, 21–27. [CrossRef]
114. Bombarda, P.; Invernizzi, C. Binary liquid metal-organic Rankine cycle for small power distributed high efficiency systems. *Proc. Inst. Mech. Eng. Part A J. Power Energy* **2015**, *229*, 192–209. [CrossRef]
115. Krasin, A.; Nesterenko, V. Dissociating Gases: A New Class of Coolants and Working Substances for Large Power Plants. *At. Energy Rev.* **1971**, *9*, 177–194.
116. Lemmon, E.W.; Bell, I.; Huber, M.L.; McLinden, M.O. *NIST Standard Reference Database 23: Reference Fluid Thermodynamic and Transport Properties-REFPROP*; Version 10.0; National Institute of Standards and Technology: Gaithersburg, MD, USA, 2018.
117. Solovyev, E.; Kuvshinov, D.; Ermakov, D.; Kuvshinov, G. Production of hydrogen and nanofibrous carbon by selective catalytic decomposition of propane. *Int. J. Hydrogen Energy* **2009**, *34*, 1310–1323. [CrossRef]
118. Dai, X.; Shi, L.; An, Q.; Qian, W. Screening of hydrocarbons as supercritical ORCs working fluids by thermal stability. *Energy Convers. Manag.* **2016**, *126*, 632 – 637. [CrossRef]
119. Tsang, W. Thermal stability of cyclohexane and 1-hexene. *Int. J. Chem. Kinet.* **1978**, *10*, 1119–1138. [CrossRef]
120. Zanetti, J.; Egloff, G. The Thermal Decomposition of Benzene. *Ind. Eng. Chem.* **1917**, *9*, 350–356. [CrossRef]
121. Invernizzi, C.M.; Iora, P.; Manzolini, G.; Lasala, S. Thermal stability of n-pentane, cyclo-pentane and toluene as working fluids in organic Rankine engines. *Appl. Therm. Eng.* **2017**, *121*, 172–179. [CrossRef]
122. Invernizzi, C.; Bonalumi, D. Thermal stability of organic fluids for Organic Rankine Cycle systems. In *Organic Rankine Cycle (ORC) Power Systems*; Macchi, E., Astolfi, M., Eds.; Woodhead Publishing: Sawston, UK, 2017; pp. 121–151.
123. Dai, X.; Shi, L.; An, Q.; Qian, W. Thermal stability of some hydrofluorocarbons as supercritical ORCs working fluids. *Appl. Therm. Eng.* **2018**, *128*, 1095 – 1101. [CrossRef]
124. Calderazzi, L.; di Paliano, P.C. Thermal stability of R-134a, R-141b, R-13I1, R-7146, R-125 associated with stainless steel as a containing material. *Int. J. Refrig.* **1997**, *20*, 381–389. [CrossRef]
125. Angelino, G.; Invernizzi, C. Experimental investigation on the thermal stability of some new zero ODP refrigerants. *Int. J. Refrig.* **2003**, *26*, 51 –58. [CrossRef]
126. Okada, K.; Tschuikow-Roux, E.; Evans, P. Single-pulse shock-tube study of the thermal decomposition of ethyl fluoride and propyl chloride. *J. Phys. Chem.* **1980**, *84*, 467–471. [CrossRef]
127. Ito, M.; Dang, C.; Hihara, E. Thermal decomposition of lower-GWP refrigerants. In Proceedings of the 15th International Refrigeration and Air Conditioning Conference at Purdue, Purdue University, West Lafayette, IN, USA, 14–17 July 2014.
128. Lees, F.P. *Loss Prevention in the Process Industries: Hazard Identification, Assessment, and Control*; Butterworth-Heinemann: Oxford, UK, 1996; Volume 1.
129. Ribeiro, N.; Casimiro, T.; Duarte, C.; Nunes da Ponte, M.; Aguiar-Ricardo, A.; Poliakoff, M. Vapor- Liquid Equilibrium and Critical Line of the CO_2+ Xe System. Critical Behavior of CO_2+ Xe versus CO_2+ n-Alkanes. *J. Phys. Chem. B* **2000**, *104*, 791–795. [CrossRef]